| Topic | Seismic source location |
|---|---|
| **Authors** | **Jens Havskov**, University of Bergen, Department of Earth Science, Allégaten 41, N-5007 Bergen, Norway, Fax: +47 55 583660, E-mail: Jens.Havskov@geo.uib.no<br>**Peter Bormann**, (formerly GFZ German Research Centre for Geosciences, 14473 Potsdam, Germany); E-mail: pb65@gmx.net<br>**Johannes Schweitzer**, NORSAR, P.O.Box 53, N-2027 Kjeller, Norway, Fax: +47 63818719, E-mail: johannes.schweitzer@norsar.no |
| **Version 2** | September, 2011; **DOI: 10.2312/GFZ. NMSOP-2_IS_11.1** |



# 1 Introduction

The exact location of any source, radiating seismic energy, is one of most important tasks in practical seismology and from time to time most seismologists have been involved in this task. The intention here is to describe the most common location methods without going into the mathematical details, which have been described in numerous textbooks and scientific papers but to give some practical advice on seismic source location. Chapter 9 gives more information about the usage of seismic arrays for seismic source location.

In the case of an earthquake, the source location is defined by its hypocenter ($x_0$, $y_0$, $z_0$) and the origin time $t_0$. The hypocenter is commonly considered to be the physical location of the starting (or initiation) point of the rupture process, usually given in longitude ($x_0$), latitude ($y_0$), and depth below the surface ($z_0$ [km]). For simplicity, the hypocenter will be labeled $x_0$, $y_0$, $z_0$ with the understanding that it can be either measured in geographical or Cartesian coordinates, i.e., in [deg] or [km], respectively. The origin time is the start time of the earthquake rupture. The epicenter is the projection of the hypocenter on the Earth's surface ($x_0$, $y_0$). When the earthquake is large, the physical dimension of the rupture zone can be several hundred square kilometers and the hypocenter can in principle be located anywhere on the rupture surface with consequences also for the position of the related epicenter on the Earth´s surface.

The hypocenter and origin time are determined by arrival times, incidence direction (backazimuth) and/or horizontal velocity of seismic phases radiated by the first break of the earthquake rupture. This is true when using any P or S phases since their propagation velocity is always larger than the rupture velocity. Therefore, P- or S-wave energy emitted from the end of a long rupture will always arrive later than energy radiated from its beginning. Standard earthquake catalogs (such as from the International Seismological Center, ISC or the National Earthquake Information Center (NEIC) of the USGS) report origin times OT and locations based primarily on arrival times of high-frequency first P-type arrivals. These OT/location parameters can be quite different from the centroid time and centroid location obtained by moment-tensor inversion of long-period waves, which may be, for really great earthquakes, even more than a minute later than OT and more than hundred kilometers off the initial hypocenter. The reason is that these centroid solutions represent the average time and location for the entire seismic moment released by the earthquake, assuming that the latter can be considered as a point source in space with a prescribed symmetric triangular moment-rate function. Yet, even this assumption does not always hold, especially for great multiple-rupture events (e.g., Chapter 3, Fig. 3.7; Kikuchi and Fukao, 1987; Tsai et al., 2005).

# 2 Single station location

In general, epicenters are determined using many seismic phase observations from different seismic stations. However, it is also possible to locate a seismic source using a single 3-component station. Since the vector of P-wave motion is polarized in the vertical plane of propagation (see Chapter 2) it can be decomposed into a vertical and a radial component of motion. This allows calculating the backazimuth **BAZ** to the epicenter (see Figure 1). The backazimuth is defined as the direction angle from the station towards the epicenter, measured clockwise from North. The radial component of P can be reconstructed from the records of the 2 horizontal seismometer components **N**(orth)-**S**(outh) and **E**(ast)-**W**(est) and the azimuth **AZI** of particle motion can be calculated via the amplitude ratio $A_E/A_N$ of the first P-phase arrival:

$$AZI = \arctan A_E/A_N. \quad (1)$$

However, eq. (1) leaves an ambiguity of 180° since the first motion (FM) polarity in the vertical component can be up or down. To get the correct **BAZ** this has to be accounted for. Only if the first motion on the vertical component of the P phase is downward, the related horizontal particle motion shows towards the epicenter and then, when AZI is measured in the first quadrant, holds **BAZ** = **AZI**. The opposite is the case when the first motion in Z is

upward, due to an outward directed motion at the source which corresponds by definition to a compressional first motion arriving at the station. In this case the radial component of the P phase motion is directed away from the hypocenter and thus **BAZ** = **AZI + 180°** (see Figure 1). For details see Table 1 in exercise EX 11.2.

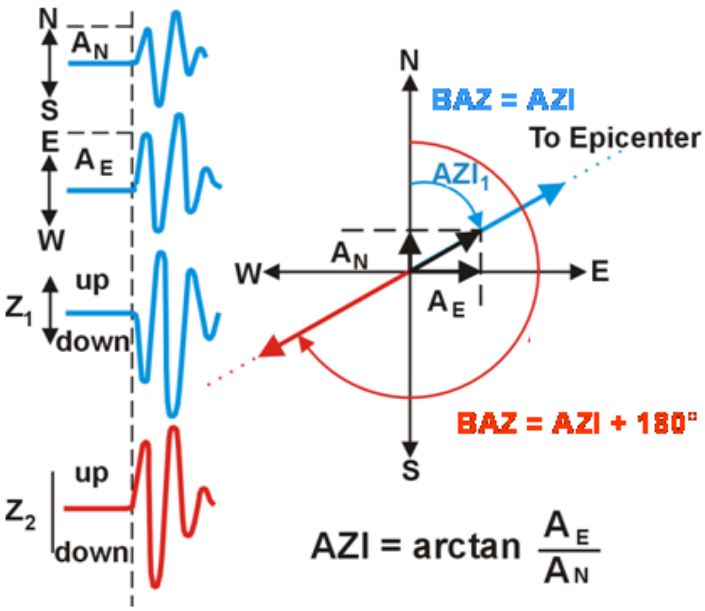


**Figure 1** Example of P-wave first motions on 3-component records (left) from which the AZI (and thereby the BAZ) and the incidence angle *i* can be derived according to Eqs. (1) and (2).

The amplitude $A_Z$ of the Z component can, together with the amplitude $A_R = (A_E^2 + A_N^2)^{1/2}$ on the radial component, also be used to calculate the *apparent angle of incidence* $i_{app} = \arctan (A_R / A_Z)$ of a P wave. However, according already to Wiechert (1907) the true incidence angle $i_{true}$ of a P wave is a function of the mean $v_P$-to-$v_S$ ratio in the crust below the station

$$i_{true} = \arcsin \left[ \frac{v_P}{v_S} \times \sin(0.5 \times i_{app}) \right], \qquad (2)$$

with the difference accounting for the amplitude distortion due to the reflection of P and SV-converted wave energy at the free surface. Knowing the incidence angle $i_o$ and the local seismic velocity $v_o$ below the observing station, we can calculate the apparent horizontal propagation velocity $v_{app}$ of this seismic phase with

$$v_{app} = v_o / \sin i_o \, . \qquad (3)$$

One should note, however, that the here described measured $i_{app}$ and thus $v_{app}$ values at a given station depend on the dominant frequency of the seismic record (see Chapter 2, Fig. 2.6). Therefore, these values are representative for the uppermost layers of the Earth corresponding to the dominant wavelength of the observed phase and not for the incidence angle and apparent horizontal velocity directly underneath the Earth's surface.

In the case of slowly emerging first P swings (e.g., Figure 6 and 8 in IS 11.4) or when analyzing narrow-band high frequency data (e.g., Chapter 4, Figs. 4.9 and 4.10, and Chapter 16, Fig. 16.25) it might not be possible to read correctly the amplitude and polarity of the first break (see Chapter 4, Figs. 4.9 and 4.10). However, the amplitude ratio between the components should remain constant, not only for the first swing of the P phase but also for the following oscillations of the same phase, provided that they are not yet distorted by superposition with laterally refracted (scattered) wave energy, as often the case in high-frequency records. If this condition is fulfilled, we can, with digital data, use the predicted coherence method (Roberts et al., 1989) to automatically calculate backazimuth as well as the angle of incidence. This is much more reliable and faster than using manually read first motion amplitudes for calculating the backazimuth from 3-component records of single stations and has become a routine practice (e.g., Saari, 1991).

In the case of seismic arrays, apparent velocity and backazimuth can directly be measured by observing the propagation of the seismic wavefront with array methods, independently from the local seismic velocities below the station (see Chapter 9). As we show later, backazimuth observations are useful in better constraining epicenter locations and in associating observations to a seismic event. Knowing the incidence angle $i_o$ at the station and implicitly the ray parameter $p = \sin i_o/v_o$ of an onset at the station helps to identify the seismic phase and to calculate the epicentral distance via the, from Earth models theoretically known, distance-dependent slowness (or ray parameter) of different seismic phases.

With a single station we have now the direction to the seismic source. The distance can also be obtained from the difference in arrival time of two phases, usually P and S. If we assume a constant velocity, and origin time $t_0$, the P- and S-arrival times can then be written as

$$t_p = t_0 + D/v_p \qquad t_s = t_0 + D/v_s \tag{4}$$

where $t_p$ and $t_s$ are the P- and S-arrival times respectively, $v_p$ and $v_s$ are the P and S velocities respectively and D is the epicentral distance for surface sources; or the hypocentral distance d for deeper sources. By eliminating $t_0$ from Equation (4), the distance can be calculated as

$$D = (t_s - t_p)\frac{v_p \cdot v_s}{v_p - v_s} \tag{5}$$

with D in km and $t_s - t_p$ in seconds. But Equation (5) is applicable only for the travel-time difference between Sg and Pg, i.e., the direct crustal phases of S and P, respectively, provided that the ratio $v_p/v_s$ does not change within the crust. Pg and Sg are first onsets of the P- and S-wave groups of local events only for distances up to about 100 – 250 km, depending on crustal thickness and source depth within the crust. Beyond these distances the phases Pn and Sn, being either head waves critically refracted at the Mohorovičić discontinuity or waves diving as body waves in the uppermost part of the upper mantle, become the first onsets (see Fig. 2.32 in Chapter 2 and Fig. 11.40 in Chapter 11). The "cross-over" distance $x_{co}$ between Pn and Pg (or Pb) can be approximately calculated for a (near) surface focus from the relationship

$$x_{co} = 2\, z_m \{(v_m - \bar{v}_p)\,(v_m + \bar{v}_p)\}^{-1/2}, \tag{6}$$

with $\bar{v}_p$ – average crustal P velocity, $v_{\underline{m}}$ – sub-Moho P velocity, and $z_m$ – crustal thickness. Inserting the rough average values of $\bar{v}_c$ = 6 km/s and $v_m$ = 8 km/s we get, as a "rule of thumb", $\mathbf{x_{co} \approx 5\ z_m}$. At smaller distances we can be rather sure that the observed first arrival is Pg. Note, however, that this "rule of thumb" is valid for surface focus only. As demonstrated with Fig. 2.40 in Chapter 2, the crossover distance is only about half as large for near Moho earthquakes and also the dip of the Moho and the direction of observation (up- or downdip) does play a role.

Examples for calculating the epicentral distance D and the origin time OT of near seismic events by means of a set of local travel-time curves for Pn, Pg, Sn and Sg (or Lg) are given in exercise EX 11.1. The lower crustal phases Pb and Sb are here less important since they may form only over a very short epicentral distance range the first arrivals of the P and S onsets. In the absence of local travel-time curves for the area under consideration one can use Equation (5) for deriving a **"rule of thumb"** for approximate distance determinations from travel-time differences Sg-Pg. For an ideal Poisson solid $v_s = v_p/\sqrt{3}$. This is a good approximation for the average conditions in the crust. With this follows from Equation (5): $D = (t_{Sg} - t_{Pg}) \times 8.0$ for "normal, medium age" crustal conditions with average $\bar{v}_p$ = 5.9 km/s, or $D = (t_{Sg} - t_{Pg}) \times 9.0$ for old Precambrian continental shields with rather large average $\bar{v}_p$ = 6.6 km/s. However, if known, the locally correct $v_p/v_s$ ratio should be used to improve this "**rule of thumb**". If the distance is calculated from the travel-time difference between Sn and Pn, another good rule of thumb is $D = (t_{Sn} - t_{Pn}) \times 10$. It may be applicable up to about 1000 km epicentral distance.

For epicentral distances between about $20^o < \Delta < 100^o$ the relationship $\Delta^o = \{(t_s - t_p)_{min} - 2\} \times 10$ still yields reasonably good epicentral distance estimates with errors < 3°, however, beyond D = 10° the use of readily available global travel-time tables such as IASP91 (Kennett and Engdahl, 1991; Kennett, 1991), SP6 (Morelli and Dziewonski, 1993), or AK135 (Kennett et al., 1995; now standard at the NEIC and the ISC) is strongly recommended for more accurate theoretical travel-time and epicentral distance calculations.

With both backazimuth and epicentral distance, the epicenter of a seismic event can be obtained by measuring off the distance along the backazimuth of approach. Finally, knowing the epicentral distance, we can calculate the P-wave travel time and thereby get the origin time using the P-arrival time (see EX 11.2 for location of teleseismic events by means of 3-component records).

It is important to mention at this point that the described single station location procedures cannot resolve the depth of a seismic event, unless the station analyst is able to surely identify depth phases in the record and determine the source depth from their time difference to the related primary phases. Otherwise, single station location is a pure epicenter and not hypocenter determination method.

# 3 Multiple station location

## 3.1 Manual location

When at least 3 stations are available, a simple manual location can be made from drawing circles (the circle method) with the center at the station locations and the radii equal to the hypocentral distances calculated from the S-P times (see Figure 2).

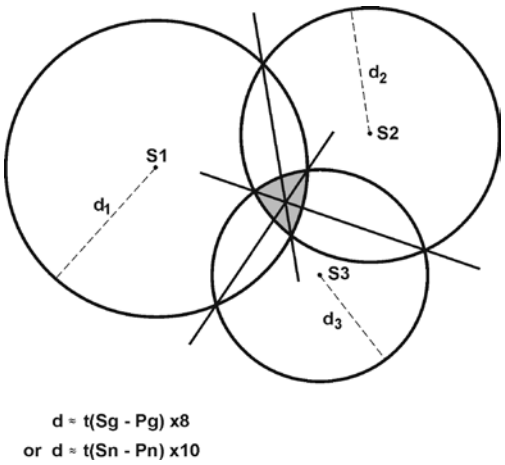


**Figure 2** Location by the "circle and chord" method. The stations are located in S1, S2 and S3. The epicenter is found within the shaded area where the circles overlap. The best estimate is the crossing of the chords, which connect the crossing points of circle pairs.

These circles will rarely cross in one point. This may be due to errors in the onset-time readings, in the assumed travel-time or related velocity model and/or that we have wrongly assumed a surface focus. In fact, $t_s - t_p$ is the travel-time difference for the hypocentral distance d, which is for seismic sources with $z > 0$ km generally larger than the epicentral distance $\Delta$ (or D). Therefore, the circles drawn around the stations with radius d will normally not be crossing at a single point at the epicenter but rather "overshooting". The amount of overshoot depends on source depth but also on not accounted lower than average velocity inhomogeneities. One should therefore fix the epicenter either in the "center of gravity" of the overlapping area (shaded area in Figure 2) or draw "chords", i.e., straight lines passing through the crossing points between two neighboring circles. These chord lines intersect in the epicenter (see Figure 1 in EX 11.1). In Section 7 of this exercise and in the animation linked with it, it is illustrated how the source depth can then be determined by iteratively minimizing the overshoot. Still other methods exist (e.g., Båth, 1979) to deal with this depth problem (e.g., the hyperbola method which uses P-wave first arrivals only and assumes a constant P-wave velocity). A detailed description of the method can be found in Pujol (2004).

During the last years Earthquake Early Warning Systems (EEWS) became more in focus and for such monitoring systems quick and reliable earthquake location methods are needed. Therefore, all graphical location algorithms became again more interesting. One approach to solve the problem is using the order of first arrival times to locate the event (Nicholson et al., 2004; Rosenberger, 2009) or applying derivatives of the hyperbola method (e.g., Font et al., 2004; Horiuchi et al., 2005; Satriano et al., 2008).

## 3.2 The Wadati diagram

With data from several stations available from a local or regional seismic source, the origin time can be determined by a very simple technique called Wadati diagram (Wadati, 1933). Using Equation (5) and eliminating Δ, the S-P travel-time difference can be calculated as

$$t_s - t_p = (v_p/v_s - 1) \times (t_p - t_0) \quad (7)$$

The observed S-P times are plotted against the absolute P time. Since $t_s - t_p$ goes to zero at the hypocenter, a straight line fit on the Wadati diagram (Figure 3) gives the origin time at the intercept with the P-arrival axis and from the slope ($v_p/v_s - 1$) of the curve, we get the ratio $v_p/v_s$. Note that it is thus possible to get a determination of both the origin time and a mean $v_p/v_s$ ratio without any prior knowledge of the crustal structure, the only assumption is that $v_p/v_s$ is constant and that the P and S phases are of the same type like Pg and Sg, Pb and Sb or Pn and Sn. Such an independent determination of these parameters can be very useful when using other location methods.

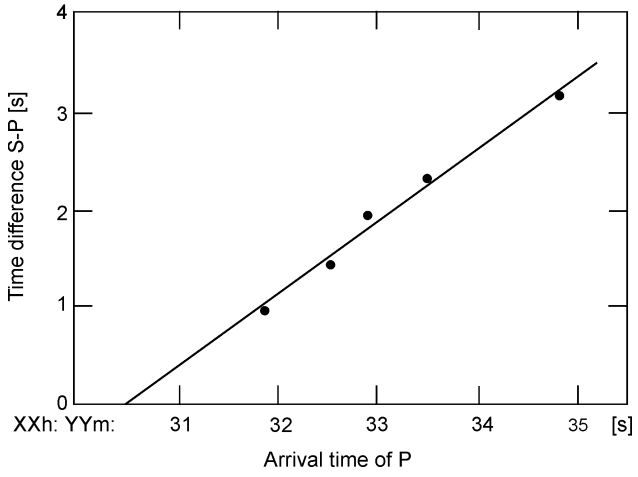


**Figure 3** An arbitrary example of a Wadati diagram. The intercept of the best fitting line through the data with the x-axis gives the origin time OT. In the given case, the slope of the line is 0.72 so the $v_p/v_s$ ratio is 1.72. The misfit of the data with this straight line indicates deviations from a constant $v_p/v_s$ ratio and/or data reading errors.

The Wadati diagram is also very useful in making independent checks of the observed arrival times. Any points not fitting reasonably well with the linear relationship might be badly identified, either by not being of the same phase type or by misreading.

## 3.3 Computer location

Manual location methods provide insight into location problems; however, in practice we use computer methods. In the following, the most common ways of calculating hypocenter and origin time by computer will be discussed.

The calculated arrival time $t_i^c$ at station i can be written as

$$t_i^c = T(x_i, y_i, z_i, x_0, y_0, z_0) + t_0 \quad (8)$$

where $T$ is the travel time as a function of the location of the station $(x_i, y_i, z_i)$ and the hypocenter. This equation has 4 unknowns, so in principle 4 arrival-time observations from at least 3 stations are needed in order to determine the hypocenter and origin time. If we have n observations, there will be n equations of the above type and the system is over determined and has to be solved in such a way that the misfit or residual $r_i$ at each station is minimized. $r_i$ is defined as the difference between the observed and calculated travel times which is the same as the difference between the observed and calculated arrival times

$$r_i = t_i^o - t^c_i \tag{9}$$

where $t_i^o$ is the observed arrival time. In principle, the problem seems quite simple. However, since the travel-time function $T$ is a nonlinear function of the model parameters, it is not possible to solve Equation (8) with any analytical methods. So even though $T$ can be quite simply calculated, particularly when using a 1-D Earth model or pre-calculated travel-time tables, the non-linearity of $T$ greatly complicates the task of inverting for the best hypocentral parameters. The non-linearity is evident even in a simple 2-D epicenter determination where the travel time $t_i$ from the point $(x, y)$ to a station $(x_i, y_i)$ can be calculated as

$$t_i = \frac{\sqrt{(x - x_i)^2 + (y - y_i)^2}}{v}, \tag{10}$$

where $v$ is the velocity. It is obvious that $t_i$ does not scale linearly with either $x$ or $y$ so it is not possible to use any set of linear equations to solve the problem and standard linear methods cannot be used. This means that given a set of arrival times, there is no simple way of finding the best solution. In the following, some of the methods of solving this problem will be discussed.

### 3.3.1 Grid search

Since it is so simple to calculate the travel times of all seismic phases to any point in the model, given enough computer power, a very simple method is to perform a grid search over all possible locations and origin times and compute the arrival time at each station (e.g., Sambridge and Kennett, 1986 and 2001; Lomax, 2005). The hypocentral location and origin time would then be the point with the best agreement between the observed and calculated times. This means that some measure of best agreement is needed, particularly if many observations are used. The most common approach is to use the least squares solution, which is to find the minimum of the sum of the squared residuals $e$ from the $n$ observations:

$$e = \sum_{i=1}^{n} (r_i)^2 \tag{11}$$

The root mean squared residual RMS, is defined as $\sqrt{e/n}$ . RMS is given in almost all location programs and commonly used as a guide to location precision. If the residuals are of similar size, the RMS gives the approximate average residual. As will be seen later, RMS only gives an indication of the fit of the data, and a low RMS does not automatically mean an accurate hypocenter determination. Generally, the precision of the computational solution, which is

based on various model assumptions, should not be mistaken as real accuracy of the location and origin time. This point will be discussed later under Section 7.

The average squared residual e/n is called the variance of the data. Formally, n should here be the number of degrees of freedom *ndf*, which is the number of observations minus the number of parameters in fit (here 4). Since *n* usually is large, it can be considered equal to the number of degrees of freedom. This also means that **RMS**$^2$ is approximately the same as the variance. The least squares approach is the most common measure of misfit since it leads to simple forms of the equations in the minimization problems (see later). It also works quite well if the residuals are caused by uncorrelated Gaussian noise. However in real problems this is often not the case. A particularly nasty problem is the existence of outliers, i.e., individual large residuals. A residual of 4 will contribute 16 times more to the misfit *e*, than a residual of 1. Using the sum of the absolute residuals as a norm for the misfit can partly solve this problem:

$$e1 = \sum_{i=1}^{n} |r_i| . \tag{12}$$

This is called the L1 norm and is considered more robust when there are large outliers in the data. It is not much used in standard location programs since the absolute sign creates complications in the equations. This is of course not the case for grid search. Therefore, most location programs will have some scheme for weighting out or truncating large residuals (see later), which can partly solve the problem.

Once the misfits (e.g., RMS) have been calculated at all grid points, one could assign the point with the lowest RMS as the 'solution'. For well-behaved data, this would obviously be the case, but with real data, there might be several points, even far apart, with similar RMS and the next step is therefore to estimate the probable uncertainties of the solution. The simplest way to get an indication of the uncertainty, is to contour the RMS as a function of x and y (2-D case) in the vicinity of the point with the lowest RMS (see Figure 4).

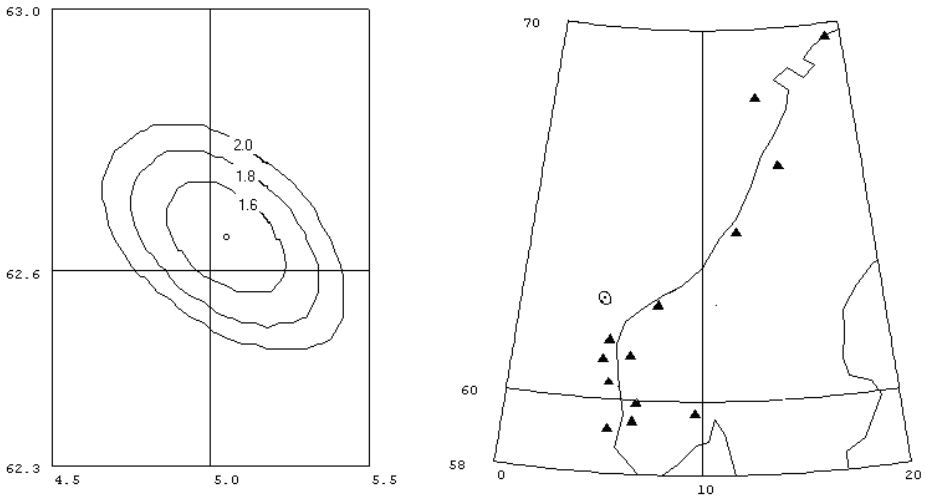


**Figure 4** Left: RMS contours (in seconds) from a grid search location of an earthquake off western Norway (left). The grid size is 2 km. The circle in the middle indicates the point with the lowest RMS (1.4 s). Right: The location of the earthquake and the stations used. Note the elongated geometry of the station distribution. Its effect on the error distribution will be

discussed in Section 4.1 below. The RMS ellipse from the figure on the left is shown as a small ellipse in the figure at right. Latitudes are degrees North and longitudes degrees East.

Clearly, if RMS is growing rapidly when moving away from the minimum, a better solution has been obtained than if RMS grows slowly. If RMS is contoured in the whole search area, other minima of similar size might be found indicating not only large errors but also a serious ambiguity in the solution. Also note in Figure 4 that networks with irregular aperture have reduced distance control in the direction of their smallest aperture but good azimuth control in the direction of their largest aperture.

An important point in all grid-search routines is the method of how to search through the possible model space. In particular for events observed at teleseismic distances the model space can be very large. Sambridge and Kennett (2001) published a fast neighborhood algorithm to use for global grid search.

### 3.3.2 Location by iterative methods

Despite increasing computer power, seismic source locations are done mainly by other methods than grid search. These methods are based on linearizing the inversion problem. The first step is to make a guess of hypocenter and origin time ($x_0$, $y_0$, $z_0$, $t_0$). In its simplest form, e.g., in the case of events near or within a station network, this can be done by using a location near the station with the earliest arrival time and using that arrival time as $t_0$. Other methods also exist (see below). In order to linearize the problem, it is now assumed that the true hypocenter is close enough to the guessed value so that travel-time residuals at the trial hypocenter are a linear function of the correction we have to make in hypocentral distance.

The calculated arrival times at station i, $t_i^c$ from the trial location are, as given in Equation (8), $t_i^c = T(x_0, y_0, z_0, x_i, y_i, z_i) + t_0$ and the travel-time residuals $r_i$ are $r_i = t_i^o - t_i^c$. We now assume that these residuals are due to the error in the trial solution and the corrections needed to make them zero are $\Delta x$, $\Delta y$, $\Delta z$, and $\Delta t$. If the corrections are small, we can calculate the corresponding corrections in travel times by approximating the travel-time function by a Taylor series and using only the first term. The residual can now be written:

$$r_i = (\partial T/\partial x_i) * \Delta x + (\partial T/\partial y_i) * \Delta y + (\partial T/\partial z_i) * \Delta z + \Delta t \qquad (13)$$

In matrix form we can write this as

$$r = G * X, \qquad (14)$$

where **r** is the residual vector, **G** the matrix of partial derivatives (with 1.0 in the last column corresponding to the source time correction term) and **X** is the unknown correction vector in location and origin time.

This is a set of linear equations with 4 unknowns (corrections to hypocenter and origin time), and there is one equation for each observed phase time. Normally there would be many more equations than unknowns (e.g., 4 stations with 3 phases each would give 12 equations). The best solution to Equation (13) or Equation (14) is usually obtained with standard least squares techniques. The original trial solution is then corrected with the results of Equation (13) or

Equation (14) and this new solution can then be used as trial solution for a next iteration. This iteration process can be continued until a predefined breakpoint is reached. Breakpoint conditions can be either a minimum residuum *r*, or a last iteration giving smaller hypocentral parameter changes than a predefined limit, or just the total number of iterations. This inversion method was first invented and applied by Geiger (1910) and is known as the 'Geiger method'. The iterative process usually converges rapidly unless the data are badly configured or the initial guess is very far away from the mathematically best solution (see later). However, it also happens that the solution converges to a local minimum and this would be hard to detect in the output unless the residuals are very large. A test with a grid search program may tell if the minimum is local, or tests could be made with several initial locations or different velocity models.

So far we have only dealt with observations in terms of arrival times. Many 3-component stations and arrays now routinely report the backazimuth $\phi$ of an arrival. It is then possible to locate events with only one station and P and S times (see Figure 1). However, the depth must be fixed. If one or several backazimuth observations are available, they can be used together with the arrival time observations in the inversion algorithm. The additional equations for the backazimuth residuals are

$$r_i^{\phi} = (\partial\phi/\partial x_i) * \Delta x + (\partial\phi/\partial y_i) * \Delta y \qquad (15)$$

Equations of this type are then added to the Equations (13) or (14). The $\Delta x$ and $\Delta y$ in Equation (15) are the same as for Equation (13), however the residuals are now in degrees. At this point it is worth to mention that backazimuth observations constrain the epicenter of an event but are independent of source depth and source time.

In order to make an overall RMS, the degrees must be 'converted to seconds' in terms of scaling. For example, in the location program HYPOCENTER (Lienert et al., 1988; Lienert, 1991; Lienert and Havskov, 1995), a 10 deg backazimuth residual was optionally made equivalent to 1 s travel time residual. Using e.g., 20 deg as equivalent to 1 s would lower the weight of the backazimuth observations. Schweitzer (2001) used in the location program HYPOSAT a different approach. In this program the measured (or assumed) observation errors of the input parameters are used to individually weight all different lines of the equation system (13) or (14) before inverting it. Thereby, more uncertain observations will contribute much less to the solution than well-constrained ones and all equations become non-dimensional.

Arrays (see Chapter 9) or single stations (see Equation (3)) cannot only measure the backazimuth of a seismic phase but also its ray parameter (or apparent velocity), which is a function of epicentral distance and source depth. Consequently, the equation systems (13) or (14) to be solved for locating an event, can also be extended by utilizing such observed ray parameters *p* (or apparent velocities) as defining data. In this case we can write

$$r_i^{p} = (\partial p/\partial x_i) * \Delta x + (\partial p/\partial y_i) * \Delta y + (\partial p/\partial z_i) * \Delta z \qquad (16)$$

Also equation (16) is independent of the source time but depends on the source depth. The partial derivatives are often very small but in some cases, in particular if an event is observed with only one seismic array, observed ray parameters give additional constraint for the event location.

Equations (13), (14) and (16) are written without discussing whether the applied velocity model is defined for a layered, flat or a spherical Earth model because they are exactly the same. Using a flat-Earth transformation (e.g., Müller, 1977) any radially symmetric Earth model can be transformed into a flat model. Travel times and partial derivatives are often calculated by interpolating in tables and in principle it is possible to use any Earth model including 2-D and 3-D models to calculate theoretical travel times. In practice, 1-D models are mostly used, since 2-D and 3-D models are normally not well enough known and the travel-time computations are much more time consuming. For local seismology, it is a common practice to specify a 1-D crustal model and calculate arrival times for each ray while for global models, an interpolation in travel-time tables such as IASP91 is the most common. As Kennett and Engdahl (1991) pointed out, the preferred and much more precise method for obtaining travel times from the IASP91 model or any other 1-D global Earth model (see DS 2.1) is to apply the tau-p algorithm developed by Buland and Chapman (1983). To calculate your own travel-time tables for local or global 1-D Earth models, the computer program LAUFZE can be downloaded for free either directly from the program list in the NMSOP-2 cover page folder *Download Programs and Files* or from NORSAR's anonymous ftp-server ftp://ftp.norsar.no/pub/outgoing/johannes/lauf/, a description of the program is annexed in PD 11.2. It allows calculating travel times for many different seismic phases and an arbitrary horizontally layered model with any combination of layers with constant velocities, gradients, or first-order discontinuities.

### 3.3.3 Example of location in a homogeneous model

The simplest location case is a source in a homogeneous medium. The arrival times can be calculated as

$$T_i = \frac{\sqrt{(x - x_i)^2 + (y - y_i)^2 + (z - z_i)^2}}{v} + t_0 , \qquad (17)$$

where v is the velocity. The partial derivatives can be estimated from Equation (17) and e.g., for x, the derivative is

$$\frac{\partial T_i}{\partial x} = \frac{(x - x_i)}{v} * \frac{1}{\sqrt{(x - x_i)^2 + (y - y_i)^2 + z^2}} . \qquad (18)$$

Similar expressions can be derived for y and z.

**Table 1** Inversion of error free data. Hypocenter is the correct location, Start is the initial location, and the location is shown for the two following iterations. The rows give the hypocentral parameters (x, y, z and $t_0$), the misfit e according to Equation (11) and the RMS value of the residuals.

| | Hypocenter | Start | 1. Iteration | 2. Iteration |
|---|---|---|---|---|
| x [km] | 0.0 | 3.0 | -0.5 | 0.0 |
| y [km] | 0.0 | 4.0 | -0.6 | 0.0 |
| z [km] | 10.0 | 20.0 | 10.1 | 10.0 |
| $T_0$ [s] | 0.0 | 2.0 | 0.2 | 0.0 |
| e [$s^2$] | | 94.2 | 0.6 | 0.0 |
| RMS [s] | | 3.1 | 0.25 | 0.0 |

Table 1 gives an example of locating an earthquake with 10 stations in a model with constant velocity (from Stein, 1991). The stations are between11 and 50 km apart from the hypocenter. The earthquake has an origin time of 0 s at the point (0, 0, 10) km. The initial location is at (3, 4, 20) km at 2 s. The exact travel times were calculated using a velocity of 5 km/s and the iterations were done as indicated above. At the initial guess, the sum of the squared residuals was 92.4 $s^2$, after the first iteration it was reduced to 0.6 $s^2$ and already at the second iteration; the 'correct' solution was obtained. This is hardly surprising, since the data had no errors. We shall later see how this works in the presence of errors.

### 3.3.4 Advanced methods

The problem of locating seismic events has during the last decade experienced a lot of attention and new procedures have been developed such as the double-difference location algorithm (Waldhauser and Ellsworth, 2000), a novel global differential evolution algorithm (Ružek and Kvasnička (2001), a probabilistic approach to location in 3-D and layered models by Lomax et al. (2000) as well as advanced grid search procedures to be applied in highly heterogeneous media (Lomax et al., 2001). Recent advances in travel-time calculations for three-dimensional structures complement these methods (e.g., Thurber and Kissling, 2000). Figure 5 shows how much the *precision* (or relative inter-event accuracy) of the locations within earthquake clusters can be improved by applying the above mentioned double-difference location algorithm. Several of these developments are summarized in a monograph edited by Thurber and Rabinowitz (2000), which also includes advances in global seismic event location procedures (Thurber and Engdahl, 2000).

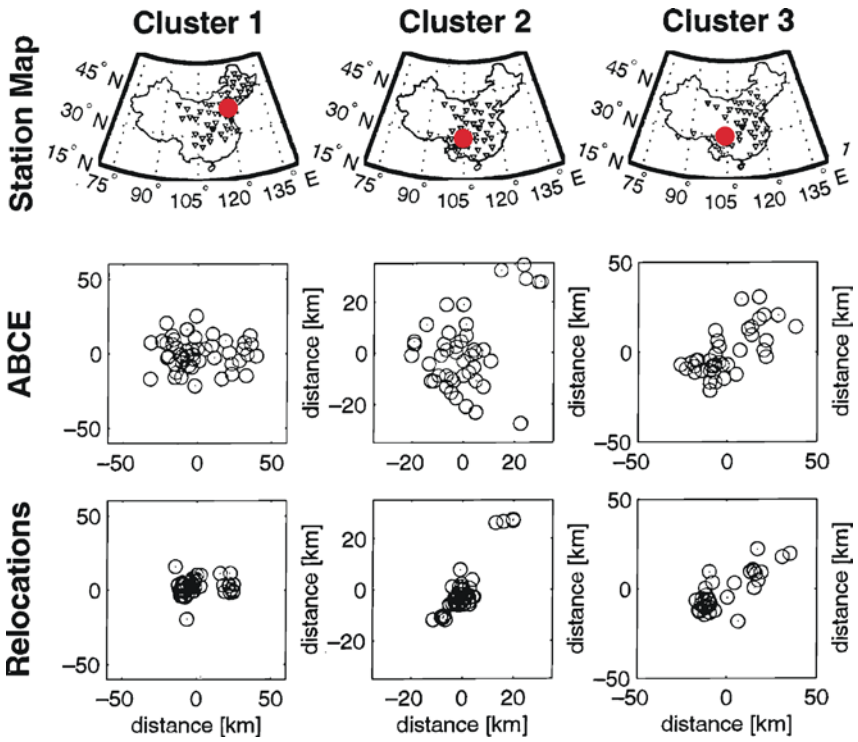


**Figure 5** Examples of improving the ABCE locations for earthquake clusters (red dots) from regional networks of seismic stations (triangles) in China by relocating the events with the double-difference location algorithm (courtesy of Paul G. Richards).

A special volume about event location in context with the special requirements for monitoring the CTBT was published by Ringdal and Kennett (2001). During the IASPEI General Assembly in Santiago de Chile (2005) a workshop had been organized about the question how the ISC location procedures can be improved. Many contributions to this workshop were later published in a special volume (Schweitzer and Storchak, 2006).

# 4 Location errors

## 4.1 Error quantification and statistics

Since seismic events are located with arrival times that contain observational errors and the travel times are calculated under the wrong assumption that the exact model is known, all hypocenter determinations will have errors. Contouring the grid search RMS (Figure 4) gives an indication of the uncertainty of the epicenter. Likewise it would be possible to make 3-D contours to get an indication of the 3-D uncertainty. The question is now how to quantify this measure. The RMS of the final solution is very often used as a criterion for 'goodness of fit'. Although it can be an indication, RMS depends on the number of stations and does not in itself give any indication of errors and RMS is not reported by, e.g., NEIC and ISC.

From Figure 4 it is seen that the contours of equal RMS are not circles. We can calculate contours within which there is a 67 % probability (or any other desired probability) of finding the epicenter (see below). We call this the error ellipse. This is the way hypocenter errors normally are represented. It is therefore not sufficient to give one number for the hypocenter error since it varies spatially. Standard catalogs from NEIC and ISC give the errors in latitude,

longitude and depth, which can also be very misleading unless the error ellipse has the minor and major axis NS or EW. In the example in Figure 4, this is not the case. Thus the only proper way to report error is to give the full specification of the error ellipsoid.

Before going into a slightly more formal discussion of errors, let us try to get a feeling for which elements affect the shape and size of the epicentral error ellipse. If we have no arrival time errors, there are no epicenter errors so the magnitude of the error (size of error ellipse) must be related to the arrival time uncertainties. If we assume that all arrival time reading errors are equal, only the size and not the shape of the error ellipse can be affected. So what would we expect to give the shape of the error ellipse? Figure 4 is an example of an elongated network with the epicenter off to one side. It is clear that in the NE direction, there is a good control of the epicenter since S-P times control the distances in this direction due to the elongation of the network. In the NW direction, the control is poor because of the small aperture of the network in this direction. We would therefore expect an error ellipse with the major axis NW as observed. Another way of understanding, why the error is larger in NW than it is in NE direction, is to look at Equation (12). The partial derivatives $\partial T/\partial x$ will be much smaller than $\partial T/\partial y$ so the $\Delta y$-terms will have a larger weight then the $\Delta x$-terms in the equations (strictly speaking the partial derivatives with respect to NW and NE). Consequently, errors in arrival times will affect $\Delta x$ more than $\Delta y$. Note that if backazimuth observations were available for any of the stations far in the North or the South of the event, this would drastically reduce the error estimate in the EW direction since $\partial\phi/\partial x$ is large while $\partial\phi/\partial y$ is nearly zero.

Changing the geometry of the stations would give another shape of the error ellipse. It is thus possible for any network to predict the shape and orientation of the error ellipses, and given an arrival error, also the size of the ellipse for any desired epicenter location. This can, e.g., be used to predict how a change in network configuration would affect earthquake locations at a given site.

In all these discussions, it has been assumed that the errors have Gaussian distribution and that there are no systematic errors like clock errors. It is also assumed that there are no errors in the theoretical travel times, backazimuths, or ray parameter calculations due to unknown structures. This is of course not true in real life; however error calculations become too difficult if we do not assume a simple error distribution and that all stations have the same arrival time error. This means, however, that such error calculations give us only an idea about the "internal" precision of the locations within the model framework on which they are based. They should not be mistaken as being true location errors (see Section 7).

The previous discussion gave a qualitative description of the errors. We will now show how to calculate the actual hypocentral errors from the errors in the arrival times and the network configuration. The most common approach to seismic source location is based on the least squares inversion and a Gaussian distribution of the arrival time errors, in which case the statistics is well understood and we can use the Chi-Square probability density distribution to calculate errors. For a particular location, $\chi^2$ can be calculated as:

$$\chi^2 = \frac{1}{\sigma^2}\sum_{i=1}^{n} r_i^2 \,, \tag{19}$$

where σ is the assumed same standard deviation of any one of the residuals and n is the number of observations. We can now look at the standard statistical tables (extract in Table 2) to find the expected value of $\chi^2$ within a given probability. As can be seen from the table, within 5% probability, $\chi^2$ is approximately the number of degrees of freedom (*ndf*), which in our case is *n-4*.

**Table 2** The percentage points of the $\chi^2$ distribution for different numbers of degrees of freedom (*ndf*)

| *ndf* | $\chi^2$ (95%) | $\chi^2$ (50%) | $\chi^2$ (5%) |
|---|---|---|---|
| 5 | 1.1 | 4.4 | 11.1 |
| 10 | 3.9 | 9.3 | 18.3 |
| 20 | 10.9 | 19.3 | 31.4 |
| 50 | 34.8 | 49.3 | 67.5 |
| 100 | 77.9 | 99.3 | 124.3 |

If e.g., an event is located with 24 stations (*ndf*=20), there is only a 5% chance that $\chi^2$ will exceed 31.4. The value of $\chi^2$ will grow as we move away from the best fitting epicenter and in the example above, the contour within which $\chi^2$ is less than 31.4 will show the error ellipse within which there is a 95 % chance of finding the epicenter. In practice, errors are mostly reported within 67 % probability, which mean with ± 1 standard deviation.

The errors in the hypocenter and origin time can also formally be defined with the variance – covariance matrix $\boldsymbol{\sigma_X^2}$ of the hypocentral parameters. This matrix is defined as

$$\sigma_X^2 = \begin{Bmatrix} \sigma_{xx}^2 & \sigma_{xy}^2 & \sigma_{xz}^2 & \sigma_{xt}^2 \\ \sigma_{yx}^2 & \sigma_{yy}^2 & \sigma_{yz}^2 & \sigma_{yt}^2 \\ \sigma_{zx}^2 & \sigma_{zy}^2 & \sigma_{zz}^2 & \sigma_{zt}^2 \\ \sigma_{tx}^2 & \sigma_{ty}^2 & \sigma_{tz}^2 & \sigma_{tt}^2 \end{Bmatrix}. \tag{20}$$

The diagonal elements are variances of the location parameters *x, y, z* and $t_0$ while the off diagonal elements give the coupling between the errors in the different hypocentral parameters. For more details, see e.g., Stein (1991). The nice property about $\boldsymbol{\sigma_X^2}$ is that it is simple to calculate:

$$\boldsymbol{\sigma_X^2 = \sigma^2 * (G^T G)^{-1}}, \tag{21}$$

where $\boldsymbol{\sigma^2}$ is the variance of the arrival times multiplied by the identity matrix and $\boldsymbol{G^T}$ is $\boldsymbol{G}$ transposed. The standard deviations of the hypocentral parameters are thus given by the square root of the diagonal elements and these are the usual errors reported. So how can we use the off diagonal elements? Since $\boldsymbol{\sigma_X^2}$ is a symmetric matrix, a diagonal matrix in a coordinate system, which is rotated relatively to the reference system, can represent it. We now only have the errors in the hypocentral parameters, and the error ellipse simply have semi axes $\sigma_{xx}$, $\sigma_{yy}$, and $\sigma_{zz}$ . The main interpretation of the off diagonal elements is thus that they define the orientation and shape of the error ellipse. A complete definition therefore requires 6 elements. Eqs. (20) and (21) also show, as stated intuitively earlier, that the shape and

orientation of the error ellipse depends only on the geometry of the network and the crustal structure whereas the standard deviation of the observations is a scaling factor as long they are equal for all observations.

The critical variable in the error analysis is therefore the arrival-time variance $\sigma^2$. This value is usually larger than it would be expected from timing and picking errors alone, however it might vary from case to case. Setting a fixed value for a given data set could result in unrealistic error calculations. Most location programs will therefore estimate $\sigma$ from the residuals of the best fitting hypocenter:

$$\sigma^2 = \frac{1}{ndf} \sum_{i=1}^{n} r_i^2 \,. \tag{22}$$

Division by *ndf* rather than by *n* compensates for the improvement in fit resulting from the use of the arrival times from the data. However, this only partly works and some programs allow setting an a priori value which is used only if the number of observations is small. For small networks this can be a critical parameter.

Recently, some studies (e.g., Di Giovambattista and Barba, 1997; Parolai et al., 2001) showed, both for regional and local seismic networks, that the error estimates ERH (in horizontal) and ERZ (in vertical direction), as given by routine location programs (e.g., in HYPOELLIPSE (Lahr, 1989 and 2003)) cannot be considered as a conservative estimate of the true location error and might lead investigators to unjustified tectonic conclusions (see also Figures 11 and 12).

## 4.2 Example of error calculation

We can use the previous error free example (see Table 1) and add some errors (from Stein, 1991). We add Gaussian errors with a mean of zero and a standard deviation of 0.1 s to the arrival times. Now the data are inconsistent and cannot fit exactly. As it can be seen from the results in Table 3, the inversion now requires 3 iterations (2 before) before the locations stop changing. The final location is not exactly the location used to generate the arrival times and the deviation from the correct solution is 0.2, 0.4, and 2.2 km for x, y, and z respectively, and 0.2 s for the origin time. This gives an indication of the location errors.

It is now interesting to compare what is obtained with the formal error calculation. Table 4 gives the variance – covariance matrix. Taking the square root of the diagonal elements we get the standard deviations of *x, y, z* and $t_0$ as 0.3, 0.3 and 1.1 km and 0.1 s, respectively. This is close to the 'true' error so the solution is quite acceptable. Also note that the RMS is close to the standard error.

**Table 3** Inversion of arrival times with a 0.1 s standard error. As in Table 1, hypocenter is the correct location, Start is the initial location, and the locations are shown after the three following iterations. e is the misfit according to Equation (11).

| | Hypocenter | Start | 1. Iteration | 2. Iteration | 3. Iteration |
|---|---|---|---|---|---|
| x [km] | 0.0 | 3.0 | -0.2 | 0.2 | 0.2 |
| y [km] | 0.0 | 4.0 | -0.9 | -0.4 | -0.4 |

| | | | | | |
|---|---|---|---|---|---|
| z [km] | 10.0 | 20.0 | 12.2 | 12.2 | 12.2 |
| $t_0$ [s] | 0.0 | 2.0 | 0.0 | -0.2 | -0.2 |
| e [$s^2$] | | 93.7 | 0.33 | 0.04 | 0.04 |
| RMS [s] | | 3.1 | 0.25 | 0.06 | 0.06 |

**Table 4** Variance – covariance matrix for the example in Table 3.

| | x | y | z | t |
|---|---|---|---|---|
| x | 0.06 | 0.01 | 0.01 | 0.00 |
| y | 0.01 | 0.08 | -0.13 | 0.01 |
| z | 0.01 | -0.13 | 1.16 | -0.08 |
| t | 0.00 | 0.01 | -0.08 | 0.0 |

The variance – covariance matrix shows some interesting features. As seen from the dialog elements of the variance – covariance matrix, the error is much larger in the depth estimate than in x and y. This clearly reflects that the depth is less well constrained than the epicenter which is quite common unless there are stations very close to the epicenter and thus $|(d-\Delta)| / \Delta >> 1$. For simplicity, we have calculated the standard deviations from the diagonal terms, however since the off diagonal terms are not zero, the true errors are larger. In this example it can be shown that the semi-major and semi-minor axis of the error ellipse have lengths of 0.29 and 0.24 km respectively, and the semi-major axis trends N22°E, so the difference from the original diagonal terms is small.

The z,t or (t,z) term, the covariance between depth and origin time, is negative, indicating a negative trade-off between the focal depth and the origin time; an earlier source time can be compensated by a larger source depth and vice versa. This is commonly observed in practice and is more prone to happen if only first P-phase arrivals are used such that there is no strong control of the source depth by P times measured at different distances.

Error calculation is a fine art, there are endless variations on how it is done and different location programs will usually give different results.

# 5 Relative location methods

## 5.1 Master event technique

The relative location between events within a certain region can often be made with a much greater accuracy than the absolute location of any of the events. This is the case when velocity variations outside the local region are the major cause of the travel-time residuals such that residuals measured at distant stations will be very similar for all of the local events. Usually, the events in the local area are relocated relative to one particularly well-located event, which is then called the **master event**.

Since Gutenberg and Richter (1937), hypocenters of closely located events have been estimated relatively to each other by choosing one of them as a master event. Later, algorithms were developed to solve the problem for larger sets of events in one common

inversion scheme (e.g., Douglas, 1967; Evernden, 1969; Dewey, 1972; Dewy and Algermissen, 1974). Today, many program packages can be found that locate large sets of events more or less closely spaced together, based on different solution strategies (e.g., Kissling et al., 1994; Pujol, 2000; Waldhauser and Ellsworth, 2000) depending on the availability of data types and research interests. It should be mentioned that the Master Event Technique can only be used when the distance to the stations is much larger than the distance between the events.

Most location programs can be used for a master event location. For this travel-time anomalies outside the source region are assumed to cause all individual station residuals after the location of the master event. By using these station residuals as station corrections, the location of the remaining events will be made relative to the master event since all relative changes in arrival times are now entirely due to changes in location within the source region. It is obvious that only stations and phases for which observations are available for the master event can be used for the remaining events. Ideally, the same combination of stations and phases should be used for all events.

## 5.2 Joint hypocenter location

In the Master Event Technique, it was assumed that true structure dependent residuals could be obtained absolutely correct from the master event, however, other errors could be present in the readings for the master event itself. A better way is to determine the most precise station residuals using the whole data set. This is what Joint Hypocenter Determination (JHD) is about (Douglas, 1967, Pujol, 2000; 2003). Instead of determining one hypocenter and origin time, we will jointly determine *m* hypocenters and origin times, and *n* station corrections. This is done by adding the station residuals $\Delta t_i^s$ to Equation (13) and writing the equations for all *m* events (index *j*):

$$r_{ij} = (\partial T/\partial x_{ij}) * \Delta x + (\partial T/\partial y_{ij}) * \Delta y + (\partial T/\partial z_{ij}) * \Delta x + \Delta t_i^s + \Delta t_j. \qquad (23)$$

The first to propose the JHD method was Douglas (1967). Since the matrix ***G*** of Equation (14) is now much larger than the 4 x 4 matrix for a single event location, efficient inversion schemes must be used. If we use e.g., 20 stations with 2 phases each for 10 events, there will be 20 *10 *2 = 400 equations and 80 unknowns (10 hypocenters and origin times, and 20 station residuals).

The relative locations obtained by the Master Event Technique or the JHD are usually more reliable than individually estimated relative locations. However, only if we have the absolute location of one of the events (e.g., a known explosion), we will be able to convert the relative locations of a Master Event algorithm into absolute locations, whereas for the JHD “absolute” locations are obtained for all events if the assumed velocity model is correct. Accurate relative locations are useful to study, e.g., the structure of a subduction zone or the geometry of an aftershocks area, which might indicate the orientation and geometry of the fault. Pujol (2000) has given a very detailed outline of the method and its application to data from local seismic networks. Figure 6 shows an example for increased location accuracy after applying JHD.

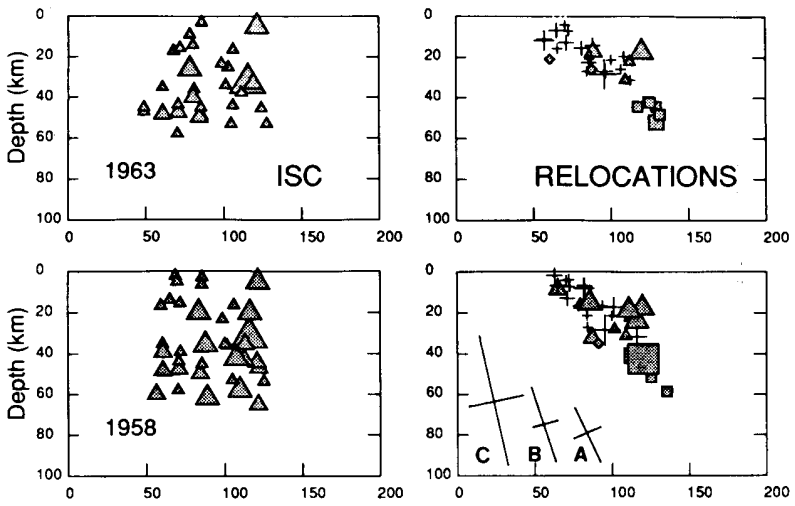


**Figure 6** Comparison of earthquake locations using the normal procedure at ISC (left) and JHD relocations (right). The events are located in the Kurile subduction zone along the rupture zones of large thrust events in 1963 and 1958. The vertical cross sections shown traverse the thrust zone from left to right. Note that the JHD solutions reduce the scatter and make it possible to define a dipping plane (from Schwartz et al., 1989).

# 6 Practical consideration in seismic source locations

This section is intended to give some practical hints on seismic source location. Different location programs, in particular for observations at local and regional distances, have been developed and are in use since many years (e.g., HYPO71 (Lee and Lahr, 1975; Lee et al., 2003), HYPOINVERSE (Klein, 1978; 1985, 2002, 2003), HYPOELLIPSE (Lahr, 1982; 2003)). This Section does not refer to any particular location program, but most of the parameters discussed can be used with the programs HYPOCENTER (Lienert et al., 1988; Lienert, 1991; Lienert and Havskov, 1995) or HYPOSAT (Schweitzer, 2001, see also PD 11.1), which can locate seismic sources at local, regional and teleseismic distances.

## 6.1 Seismic phases

For the IASPEI recommended seismic phase-naming conventions see IS 2.1 or Storchak et al. (2003). The most unambiguous seismic phase to pick is usually the first P phase. Such P phases are the main phase observations used for most teleseismic locations. For seismic events at local and regional distances, usually S phases are also used. Using phases with different seismic velocities and/or slownesses has the effect of better constraining the distances and there is then less trade-off between depth and origin time or epicenter location and origin time if the epicenter is outside the network. The focal depth is best controlled (with no trade-off between depth and origin time) when seismic phases are included in the location procedure, which have a different sign of the partial derivative $\partial T/\partial z$ in Equation (13) such as for very locally observed direct up-going Pg (positive) and Pn (negative) (see Section 6.3 Hypocentral depth and Figure 9). In general, it is thus an advantage to use as many different phases as possible under the assumption that they are correctly identified. Schöffel and Das (1999) gave a striking example (see Figure 7). But one very wrong phase can throw off an

otherwise well constrained solution. This highlights the crucial importance of the capability of the observatory personnel to recognize and report such phases during their routine seismogram analysis.

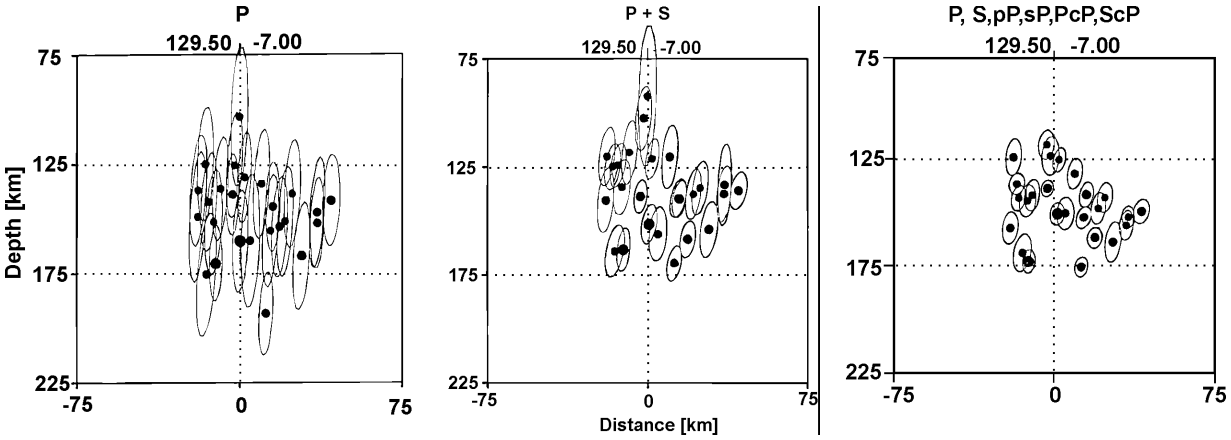


**Figure 7** Examples of significant improvement of hypocenter location for teleseismic events by including secondary phases. Left: hypocenter locations using only P phases; middle: by including S phases; right: by including also depth phases and core reflections with a different sign of $\partial T/\partial z$ (modified from Schöffel and Das, J. Geophys. Res., Vol. 104, No. B6, page 13, Figure 2; © 1999, by permission of American Geophysical Union).

Engdahl et al. (1998) used the entire ISC database to relocate more than 100,000 seismic events. They used not only a new scheme to associate correctly secondary phases, they also systematically searched for pwP onsets in the case of subduction-zone events to get better depth estimates, and they used a more modern global Earth model (AK135) to avoid the known problems with the Jeffreys-Bullen tables (Jeffreys and Bullen, 1940; 1948; 1958; 1967; 1970). With all these changes the authors reached a far more consistent distribution of hypocenters (in particular for subduction zones) and sharper picture of global seismicity. From data year 2006 on, the ISC is using model AK135 instead of the Jeffreys-Bullen tables in its bulletin productions.

The majority of location programs for local earthquakes use only first arrivals (e.g., HYPO71, Lee and Lahr, 1975). This is good enough for many cases. In some distance ranges, Pn is the first arrival, and it usually has small amplitudes. This means that the corresponding Sn phase, which is then automatically used by the program, might have also very small amplitudes and is not recognized, while actually the phase read is Sg or Lg instead. Since the program automatically assumes a first arrival, a wrong travel-time curve is used for the observed phase, resulting in a systematic location error. This error is amplified by the fact that the S phase, due to its low velocity, has a larger influence on the location than the P phase. It is therefore important to use location programs where all crustal phases can be specified.

Schweitzer (2001) developed an enhanced routine to locate both local/regional and teleseismic events, called HYPOSAT. The program runs with global Earth models and user defined horizontally layered local or regional models with layers of arbitrary velocity gradients. It provides the best possible hypocenter estimates of seismic sources by using travel-time differences between the various observed phases besides the usual input parameters such as arrival times of first and later onsets (complemented by backazimuth and ray parameters in the case of array data or polarization analyses). If S observations are also

available, preliminary origin times are estimated by using the Wadati approach (see Figure 3 in Section 3.2). An initial epicenter with a priori uncertainties can be estimated by calculating the intersection of all backazimuth observations. By relocating events with real data Schweitzer could show that HYPOSAT solutions have the smallest errors when, besides the absolute onset times the travel-time differences of all available primary and secondary phase readings are also taken into account. The most advanced version of HYPOSAT can be downloaded for free either directly from the program list in the NMSOP-2 cover page folder *Download Programs & Files* or from NORSAR's anonymous ftp-server ftp://ftp.norsar.no/pub/outgoing/johannes/hyposat/ and a detailed program description is given in PD 11.1.

## 6.2 Initial location

Iterative location programs often start with an initial location at a point near the station recording the earliest arrival. This is good enough for most cases, particularly when the station coverage is good and the epicenter is near or within the network. However, this can also lead to problems when using least squares techniques, which converge slowly or sometimes not at all for events outside the limits of a regional network (Buland, 1976). Another possibility is that the solution converges to a local minimum, which might be far from the correct solution. For small-elongated networks, two potential solutions may exist at equal distances from the long axis. An initial location close to the station with the earliest arrival can then bias the final solution to the corresponding side of such a network. Although this bias usually is on the correct side, any systematic error in the earliest-arrival station's time can have a disproportionately strong effect on the final location. Thus in many cases, it is desirable to use a better start location than the nearest station. There are several possibilities:

a) in many cases the analyst knows by experience the approximate location and can then manually give an initial location; most programs have this option;
b) similar phases at different stations can be used to determine the apparent velocity and backazimuth of a plane wave using linear regression on the arrival times (e.g., using the network as a seismic array, see Chapter 9). With apparent velocity and/or S-P times, an estimate of the initial location can be made. This method is particularly useful when locating events far away from the network (regionally or globally);
c) backazimuth information is frequently available from 3-component stations or seismic arrays and can be used as under b;
d) if backazimuth observations are available from different stations, an initial epicenter can be determined by calculating the intersection of all backazimuth observations;
e) S-P and the circle method can be used with pairs of stations to get an initial location;
f) the Wadati approach can be used to determine an initial source time.

The initial depth is usually a fixed parameter and set to the most likely depth for the region. For local earthquakes usually a depth range of 10-20 km is used, while for distant events, the initial depth was often set to 33 km, which is the crustal thickness in the Jeffreys-Bullen spherical Earth model. If depth phases, e.g., pP are available for distant events, these phases can be used to set or fix the depth (see next section).

## 6.3 Hypocentral depth

The hypocentral depth is the most difficult parameter to determine due to the fact that the travel-time derivative with respect to depth changes very slowly as function of depth (see Figure 8) unless the station is very close to the epicenter. In other words, the depth can be moved up and down without changing the travel time much. Figure 8 shows a shallow (ray 1) and a deeper event (ray 2). It is clear that the travel-time derivative with respect to depth is nearly zero for ray 1 but not for ray 2. In this example, it would thus be possible to get a depth estimate for the deeper event but not for the shallower one. Unfortunately, at larger distances from the source, most rays are more like ray 1 than ray 2 and locations are therefore often made with a fixed 'normal' start depth. Only after a reliable epicenter is obtained will the program try to iterate for the depth. Another possibility is to locate the event with several initial depths and then use the depth that gives the best fit to the data. Although one depth will give a best fit to all data, the depth estimate might still be very uncertain and the error estimate must be checked.

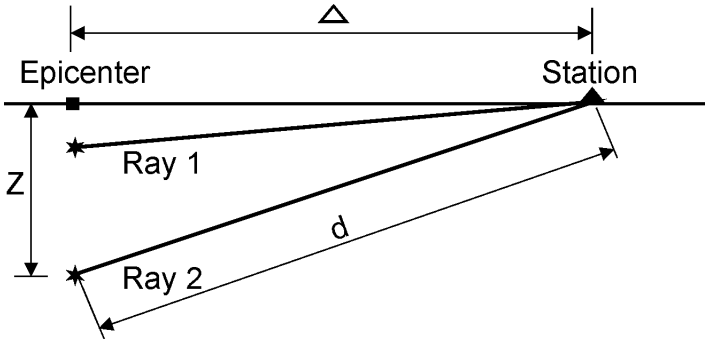


**Figure 8** The depth – distance trade off in the determination of focal depth.

For teleseismic events, the best way to improve the depth determination is to include readings from the so-called depth phases (e.g., Gutenberg and Richter, 1936 and 1937; Engdahl et al., 1998) such as pP, pwP (reflection from the ocean free surface), sP, sS or similar but also reflections from the Earth's core like PcP, ScP or ScS (see Figure 7). The travel-time differences (i.e., depth phase-direct phase) as pP-P, sP-P, sS-S and pS-S are quite constant over a large range of epicentral distances for a given depth so that the depth can be determined nearly independently of the epicentral distance. Another way of getting a reliable depth estimate for teleseismic locations is to have both near and far stations available. In particular, event observations from local and regional stations together with PKP observations have been used together for this purpose. However, this is unfortunately not possible for many source regions and small magnitude events.

For local events, a rule of thumb is that at least several near stations should not be further away than 2 times the depth in order to get a reliable estimate (Figure 8). This is very often not possible, particularly for regional events. At a distance of more than 2 × depth, the depth-depending partial derivative changes very little with depth if the first arriving phase is the more or less horizontally propagating Pg. But at distances where the critically refracted (so-called head-waves) Pb or Pn arrive, there is again some sensitivity to depth due to the more steeply down going rays of Pb or Pn (Figure 9) and because of the different sign of the partial derivatives of their travel times with depth, which is negative for Pn and positive for Pg. Thus, if stations are available at distances where both direct and refracted rays are first arrivals, reasonably reliable depth solutions might be obtained. An even better result one gets when both Pg and Pn arrivals can reliably be picked at the same station. The accuracy of the

hypocenter location is then comparable to using P and pP for teleseismic events. Yet, correct identification of secondary P phases is often difficult and a wrong identification might make matters worse.

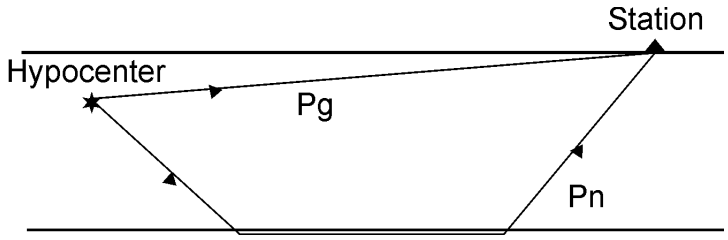


**Figure 9** Example of both Pg and Pn rays in a simplified, single layer crustal model.

The depth estimate using a layered crustal model remains problematic even with a mix of phases. In checking catalogs with local earthquakes, it will often be noted that there is a clustering of hypocenters at layer boundaries. This is caused by the discontinuities in the travel-time curves of the direct phase Pg as a function of depth at layer boundaries (see Figure 10 as an example). The Pg-travel time suddenly decreases when the hypocenter crosses a boundary (here Moho) since a larger part of the ray suddenly is in a higher velocity layer, while the Pn-travel time continuously decreases as the depth increases as long as the event is still within the crust. This gives rise to the discontinuities in the Pg-Pn travel-time curve. So one Pn-Pg travel-time difference is not enough to ensure a reliable depth estimate, several such phase arrivals must be available.

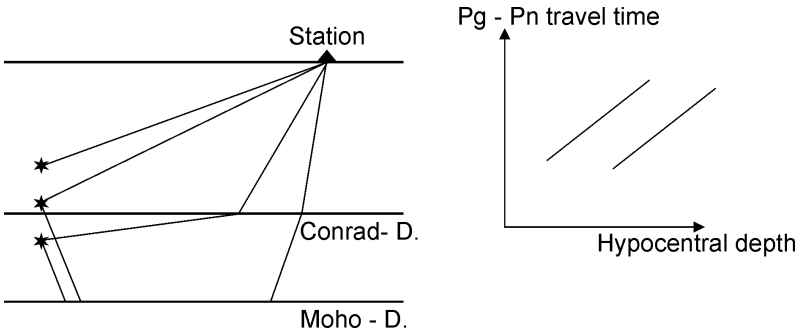


**Figure 10** Simplified two-layer crustal model of ray paths of Pg and Pn phases (left). On the right-hand panel the travel-time difference Pg-Pn as a function of depth is qualitatively sketched. It is assumed that the distance is large enough for Pn to be the first arrival.

Even when several Pg, Pb (very seldom) and Pn phases are available, depth estimates still remain a problem at regional distances due to the uncertainty in the crustal models. Since the depth estimates critically depend on accurate travel-time calculations for these phases, small model uncertainties can quickly throw off the depth estimate.

Many location programs give the RMS of the travel-time residuals in a grid around the calculated hypocenter. In addition to the error estimates, this gives an idea about the accuracy and thus a local minimum might be found. A more direct way of estimating the quality of the depth estimate is to calculate the RMS as a function of depth in order to check if a local

minimum has been reached. This is particularly relevant for crustal earthquakes at shallow depth and can also be used as a complementary tool for discriminating better between quarry blasts and earthquakes.

## 6.4 Outliers and weighting schemes

The largest residuals have a disproportionally large influence on the fit of the arrival times due to the commonly used least squares fit. Most location programs will have some kind of residual weighting scheme in which observations with large residuals are given lower or even no weight. Bisquare weighting is often used for teleseismic events (Anderson, 1982). The residual weighting works very well if the residuals are not extreme since the residual weighting can only be used after a few iterations when the residuals are already close to the final ones. Individual large residuals can often lead to completely wrong solutions, even when 90% of the data are good; residual weighting will not help in these cases. Some programs will try to scan the data for gross errors (like minute errors) before starting the iterative procedure. If an event has large residuals, try to look for obvious outliers. A Wadati diagram can often help in spotting bad readings for local events (see Figure 3 in Section 6.2).

The arrival-time observations by default will always have different weights in the inversion. A simple case is that S waves may have larger weights than P waves due to their lower velocities. An extreme case is the T wave (a guided wave in the ocean), which with its low velocity (1.5 km/s) can completely dominate the solution. Considering that the accuracy of the picks is probably best for the P waves, it should be natural that P arrivals have more importance than S arrivals in the location. However, the default parameter setting in most location programs is to leave the original weights unless the user actively changes them. It is normally possible to give *a priori* for all S phases a lower weight and in addition, all phases can be given individual weights, including being totally weighted out.

When working with local seismic sources, the nearest stations will usually provide the most accurate information due to the clarity of the phases. In addition, uncertainty in the local model has less influence on the results at short distances than at large distances; this is particularly true for the depth estimate. It is therefore desirable to put more weight on data from near stations than on those from distant stations and this is usually done by using a distance weighting function of

$$w_d = \frac{x_{far} - \Delta}{x_{far} - x_{near}}, \tag{24}$$

where $\Delta$ is the epicentral distance, $x_{near}$ is the distance to which full weight is used and $x_{far}$ is the distance where the weight is set to zero (or reduced). The constants $x_{near}$ and $x_{far}$ are adjusted to fit the size of the network; $x_{near}$ should be about the diameter of the network, and $x_{far}$ about twice $x_{near}$. For a dense network, $x_{near}$ and $x_{far}$ might be made even smaller for more accurate solutions.

## 6.5 Ellipticity of the Earth

Until now we only assumed that the model used for calculating distances or travel times is either a flat model for local or regional events or a standard spherical model of the Earth for teleseismic events. However, the Earth is neither a sphere nor a flat disk but an ellipsoid symmetrical to its rotation axis. It was Gutenberg and Richter (1933) who first pointed out that the difference between a sphere and an ellipsoid must be taken into account when calculating epicentral distances and consequently also the travel times of seismic phases. Therefore, they proposed the usage of geocentric coordinates instead of geographic coordinates to calculate distances and angles on the Earth. Because of the axially symmetrical figure of the Earth, the geocentric longitude is identical to the geographic longitude. To convert a geographic latitude $lat_g$ into a geocentric latitude $lat_c$ one can use the following formula:

$$lat_c = \arctan((1-(6378.136-6356.751)/6378.136)^2 * \tan lat_g)\,. \qquad (25)$$

With this formula all station latitudes have to be converted before an event location and after the inversion, the resulting geocentric event latitude has to be converted back by applying the inverse equation

$$lat_g = \arctan(\tan lat_c /(1-(6378.136-6356.751)/6378.136)^2)\,. \qquad (26)$$

With this procedure all angle calculations related to an event location are done for a sphere. The calculated distances are measured in degrees and to convert them into km, one has to use the local Earth radius $R_{loc}$:

$$R_{loc} = \sqrt{(6378.136 * \cos lat_c)^2 + (6356.751 * \sin lat_c)^2}\,. \qquad (27)$$

This value has then to be applied for converting a distance $D$ measured in degrees into a distance measured in km, or vice versa:

$$D[km] = \frac{2\pi * R_{loc}}{360} * D[\deg] \qquad \text{or} \qquad D[\deg] = \frac{360}{2\pi * R_{loc}} * D[km] \qquad (28)$$

All standard Earth models are defined for a spherically symmetrical Earth with a mean radius of 6371 km. Therefore the standard tables also contain travel times calculated for a sphere. Bullen (1937, 1938, 1939) was the first to calculate latitude-depending travel-time corrections (ellipticity corrections) to be used together with travel-time tables for a spherical Earth. Later work on this topic was done by Dziewonski and Gilbert (1976) and Dornboos (1988b). Kennett and Gudmundsson (1996) published a set of ellipticity corrections for a large number of seismic phases calculated applying the spherical Earth model AK135.

In conclusion: to get the theoretical travel time for an event in teleseismic or regional distance, one has first to calculate the geocentric epicentral distance, then use travel-time tables as calculated for a spherical Earth model, and finally apply the latitude (event and station!) dependent ellipticity correction. Most location routines automatically apply the described methods and formulas but it is important to check this in detail and eventually to change a location program.

## 6.6 Importance of the velocity model

In this context the importance of the model assumptions underlying the location procedure has to be emphasized. The chosen 1-D regional velocity model has a strong influence on the location of seismic sources (e.g., Kennett, 1992) and many studies have shown (e.g., Kissling, 1988) that the accuracy of locating hypocenters can even be more improved by using station corrections in addition to a well-constrained global 1-D velocity. However, Spallarossa et al. (2001) showed that in strongly heterogeneous local areas even a 1-D model with station corrections does not significantly improve the accuracy of the location parameters. High-precision location in such cases can only be achieved by using a 3-D model. This is particularly true for locating earthquakes in volcanic areas (see Lomax et al., 2001).

Smith and Ekström (1996) investigated the improvement of teleseismic event locations by using a 3-D Earth model. They came to the conclusion that it "... offers improvement in event locations over all three 1-D models with, or without, station corrections." For the explosion events, the average mislocation distance is reduced by approximately 40%; for the earthquakes, the improvements are smaller. Corrections for crustal thickness beneath source and receiver are found to be of similar magnitude to the mantle corrections, but use of station corrections together with the 3-D mantle model provide the best locations. Also Chen and Willemann (2001) carried out a global test of seismic event locations using 3-D Earth models. Although a tighter clustering of earthquakes in subduction zones was achieved by using a 3-D model rather than using depth from the ISC Bulletin based on 1-D model calculations, they concluded that the clustering was not as tight as for depths computed by Engdahl et al. (1998) who used depth phases as well as direct phases. Thus, even using the best available global 3-D models can not compensate for the non-use of depth phases and core reflections in teleseismic hypocenter location (see Figure 7).

An example case for the improved location of local earthquakes is given in Figures 11 and 12. The upper panel in Figure 11 shows the initial epicenter locations of aftershocks of the Cariaco earthquake (Ms = 6.8) on July 9, 1997 in NE Venezuela based on an averaged 1-D crustal velocity model. The mean location error (i.e., the calculated *precision* with respect to the assumed model) was about 900 m. On average, the aftershocks epicenters occurred about 2 to 3 km north of the surface fault trace.

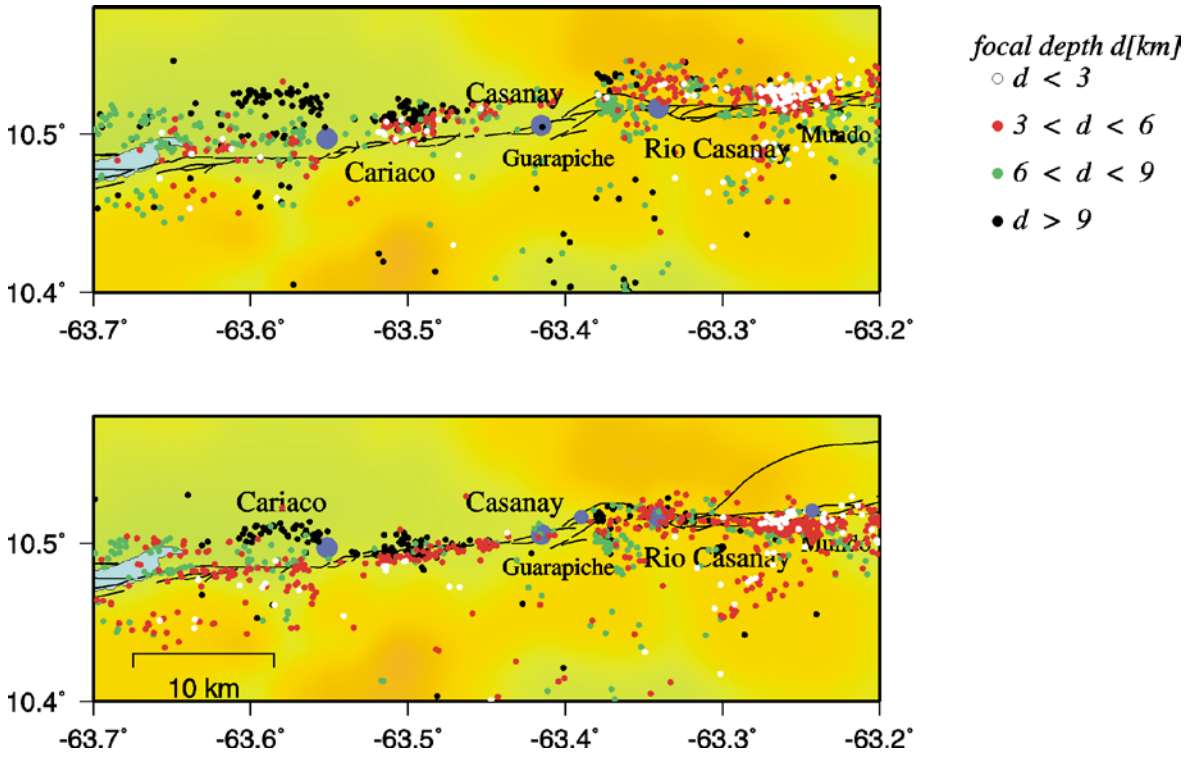


**Figure 11** Epicentral distribution of aftershocks of the Cariaco earthquake (Ms=6.8) on July 9, 1997 in NE Venezuela. Top: results from HYPO71 based on a one-dimensional velocity-depth distribution. Bottom: Relocation of the aftershocks on the basis of a 3-D model derived from a tomographic study of the aftershock region (courtesy of M. Baumbach (†), H. Grosser and A. Rietbrock).

A detailed tomographic study revealed lateral velocity contrasts of up to 20% with higher velocities towards the north of the El Pilar fault (Figure 12). Relocating the events with the 3-D velocity model the epicenters were systematically shifted southward by about 2 km and now their majority aligned rather well with fault traces mapped before the earthquake as well as with newly ruptured fault traces (Figure 11, lower panel). Also in the cross sections the data scatter was clearly reduced so that closely spaced outcropping surface faults could be traced down to a depth of more than 10 km. These results point to the fact that in the presence of lateral velocity inhomogeneities epicenter locations are systematically displaced in the direction of higher velocities. We will look into this problem more closely in Section 7.

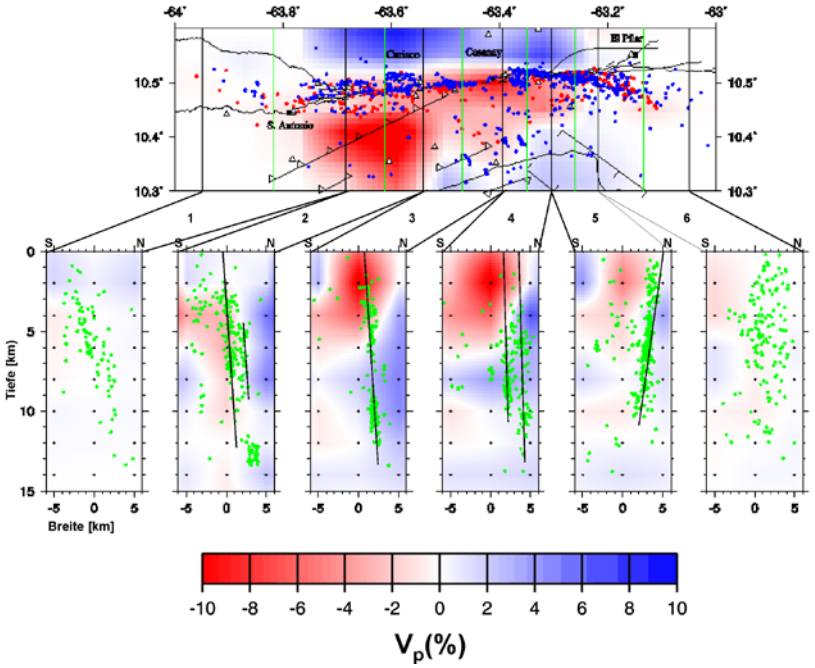


**Figure 12** 3-D distribution of the P-wave velocity in the focal region of the 1997 Cariaco earthquake as derived from a tomographic study. The horizontal section shows the velocity distribution in the layer between 2 km and 4 km depth. Red and blue dots mark the epicenters of the aftershocks. The red ones were chosen because of their suitability for the tomography. The six vertical cross sections show depth distributions of the aftershocks (green dots) together with the deviations of the P-wave velocity from the average reference model. The depth range and the lateral changes of fault dip are obvious (courtesy of M. Baumbach(✞), H. Grosser and A. Rietbrock).

# 7 Internal and external (real) accuracy of locations

For decades the international data centers have located earthquakes world-wide by means of the 1-D Jeffreys-Bullen velocity model of the Earth and Jeffreys-Bullen travel-time tables (Jeffreys and Bullen, 1940; 1948; 1958; 1967; 1970) without external control of the accuracy of such solutions by independently checking them with similarly strong events of exactly known position and origin time. Therefore, the question has remained open for a long time as to whether these calculated location errors were real or just the minimized average errors for the best fitting solutions to the observed data based on model assumptions with respect to the validity of the velocity model, the non-correlation of the various parameters to be determined and the Gaussian distribution of both the model errors and the data reading errors. If the latter is the case then the calculated errors are no measure of the real accuracy of the calculated location and origin time but rather a measure of the internal precision of fitting best the data to the used model.

In order to investigate this in more detail, Bormann (1972a and b) looked into the travel-time errors reported by the international data centers for the German seismological observatory Moxa (MOX) for earthquakes in different regions of the world. As an example, he got for the same data set of events from the Kurile Islands the mean residual $\overline{\delta t}_p$ = + 0.16 s and a standard deviation $\sigma = \pm 0.65$ s when referring the MOX onset-time readings to the locations

published by the U.S. Coastal and Geodetic Survey (USCGS, World Data Center A, WDC A) and $\bar{\delta}t_p = +0.35$ s with $\sigma = \pm 1.1$ s when referring to the locations published by the Academy of Sciences of the Soviet Union (ANUSSR, World Data Center B, WDC B) which used the same Jeffreys-Bullen travel-time tables as the USCGS. Thus, the travel-time (or onset-time reading) errors calculated by the data centers for seismic stations are not real errors of these stations or their readings but depend on the number and distribution of stations used by these centers in their location procedure. And these were rather different for WDC A and WDC B. While the USCGS used the data of a worldwide station network, ANUSSR based its locations on the station network of the former Soviet Union and East European countries and these "looked at" events outside Eurasia from a much narrower azimuth and distance range. But this is equivalent to the discussion related to Figure 4. Although the mean station residuals calculated by these two data centers for the considered region were not significantly different and not far from zero, their systematic mislocations with respect to "ground truth" locations such as those of underground nuclear explosions (Herrin and Taggart, 1968; Bormann, 1972a; Engdahl et al., 1998) reached in subduction zones with large lateral velocity inhomogeneities several 10 km and were larger for the network with a limited azimuthal coverage. Therefore, the ISC waits for one to two years before running its final location procedure. This allows collecting as many seismic phase readings as possible from worldwide distributed seismological observatories and thus assures the best geographic coverage for each seismic event.

What is the reason for this systematic mislocation, which usually remains unrecognized unless one locates strong independently controlled sources of exactly known source parameters and origin time? Figure 13 shows some hypothetical earthquakes at different depth on a vertically dipping fault. It separates two half-spaces with different wave propagation velocity $v_2 > v_1$. This is a realistic model for parts of the San Andreas Fault. The lateral velocity difference across the fault may be as large as 5 to 7 %. S1 and S2 may be two stations at the same hypocentral distances from the events. But because of $v_2 > v_1$ the onset time $t_2$ at S2 is earlier (travel-time shorter) than for $t_1$ at S1. Running the location procedure with the common residual minimization on the assumption of a laterally homogeneous velocity model will result in hypocentral distances $d_2(h) < d_1(h)$. Since the difference increases with depth, the hypocenters are not only offset from the real fault but seem to mark even a slightly inclined fault, which is not the case.

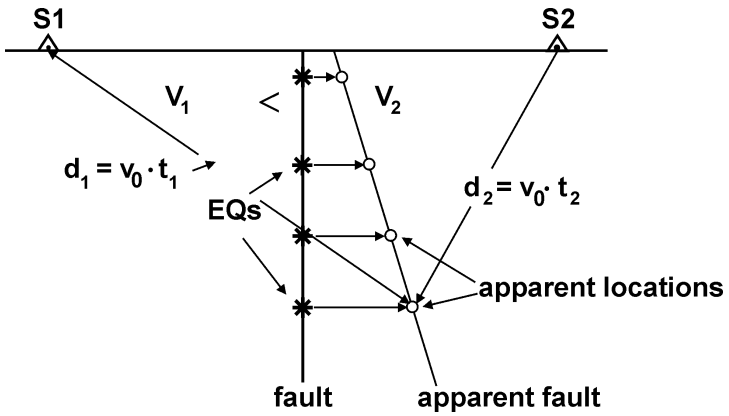


**Figure 13** Illustration of the systematic mislocation of earthquakes along a fault with strong lateral velocity contrast. $v_o$ is the assumed model velocity with $v_2 > v_o > v_1$.

From this hypothetical example we learn that locations based on 1-D velocity models in the presence of 2-D or 3-D velocity inhomogeneities will be systematically shifted in the direction of increasing velocities (or velocity gradients), the more so, the less the station distribution controls the event from all azimuths. This is precisely the cause for the above mentioned larger systematic mislocations of WDC B as compared to WDC A. While the latter localizes events using data from a global network, the former used solely data from the former Soviet and East European territory, i.e., stations which view the Aleutian Islands from only a narrow azimuth range. The direction of systematic mislocation of both centers to the NW agrees with the NW directed subduction of the Pacific plate underneath the Aleutians. According to Jacob (1972) this cold lithospheric plate has 7 to 10% higher P-wave velocities than the surrounding mantle. A study by Lienert (1997) also addresses this problem of assessing the reliability of seismic event locations by using known nuclear tests.

The above discussion illustrates that we have to differentiate between the *precision* and the *accuracy* of locations (for definition of these terms see also the Glossary) and highlights the utmost importance of the general availability and easy accessibility of so-called seismic reference events with very well known hypocenter coordinates and origin time. They are needed for tomographic studies, the derivation of improved local, regional and global velocity models, the calibration and quality assessment of seismic network and array location procedures and other related issues. Such events may be chemical or nuclear underground explosions, which are commonly known exactly, or earthquakes that have been precisely located by available dense local networks. Such reference events can be considered as independent “ground truth” (GT) data. They are classified according to the accuracy with which the event coordinates are known in terms of integer values of kilometer (GT0, GT1, GT2, GT5, GT10). GT0 to GT2 data are available only for chemical and underground nuclear explosions, GT5 and larger mostly for earthquakes.

For many years the IASPEI Commission on Seismic Observation and Interpretation (CoSOI) had entrusted a Working Group with the elaboration of guidelines for the identification, collection and quality assessment as well as the initial compilation of a world-wide listing of such events. Meanwhile, the International Seismological Centre (ISC) has established a website data base of reference earthquakes and explosions for which hypocenter information is known with high confidence and which were associated with seismic signals that have been recorded at regional and/or teleseismic distances (see http://www.isc.ac.uk/GT/index.html ). On this website one finds the actual global IASPEI Reference Event List and map. As of summer 2011 it comprised the following numbers of GT events: GT0 – 650, GT1 – 367, GT2 – 123, GT5 – 6195 (out of which about 6000 are earthquakes). Through this website one can also submit new information about reference events. IASPEI encourages the scientific community to submit to the ISC such reference event information using the IASPEI developed guidelines for identifying candidate events and assessing their quality.

How to identify and collect such ground truth events is described in detail in IS 8.6, and IS 8.5 gives more details about the criteria for assessing the accuracy and reliability of locations depending on the geometry and azimuthal distribution of reporting stations, specifically about the GT5 criteria at 90% and 95% confidence level for local networks as defined by Engdahl et al. (2001), Bondar et al. (2004), and Bondár and McLaughlin (2009), respectively. These criteria are now operationally applied in the authoritative location scheme of the European-Mediterranean Seismological Centre (EMSC; http://www.emsc-csem.org) and its real time information services. In this scheme locations are considered to be accurate when they fulfill the GT5 criteria and additionally as reliable if they can be reproduced to within 15 km when

applying different location procedures and velocity models to the same data set. To expect more accurate routine earthquake locations based on regional and common local network data is hardly realistic for earthquakes with magnitudes below 6 and questionable anyway for earthquakes with magnitudes above 7 and thus linear rupture dimensions ranging from several 10 to several 100 kilometers.

## Acknowledgments

Some of the preceding text has followed a similar description in Shearer (1999). Several figures and ideas have also been taken from Stein (1991), Lay and Wallace (1995), Schöffel and Das (1999). Thanks go to M. Baumbach, H. Grosser and A. Rietbrock for making Figures 11 and 12 available and to R. E. Engdahl for critical proof reading and valuable suggestions which helped to improve the text and to complement the references.

## References

Anderson, K. R. (1982). Robust earthquake location using M-estimates, *Phys. Earth. Plan. Inter.*, **30**, 119-130.

Båth, M. (1979). Introduction to seismology. *Birkhauser Verlag*, Basel, 428 pp.

Bondár I. and McLaughlin, K. L. (2009). A new ground truth data set for seismic studies. *Seismol. Res. Lett.*, **80**(3), 465-472

Bondár, I., Myers, S. C., Engdahl, E. R., and Bergman, E. A. (2004). Epicenter accuracy based on seismic network criteria. *Geophys. J. Intern.*, **156**, 483–496; doi10.1111/j.1365-246X.2004.02070.x.

Bormann, P. (1972a). A study of travel-time residuals with respect to the location of teleseismic events from body-wave records at Moxa station. *Gerl. Beitr. Geophys.*, **81**, 117-124.

Bormann, P. (1972b). A study of relative frequencies of body-wave onsets in seismic registrations of the station Moxa. In: Seismological Bulletin 1967, Station Moxa (MOX). *Akademie-Verlag*, Berlin 1972, 379-397

Buland, R. (1976). The mechanics of locating earthquakes, *Bull. Seism. Soc. Am.*, **66**, 173-187.

Buland, R., and Chapman, C. (1983). The computation of seismic travel times. *Bull. Seism. Soc. Am.*, **73**, 1271-1302.

Bullen, K. E. (1937, 1938, 1939). The ellipticity correction to travel-times of P and S earthquake waves. *Montl. Not. R. Astr. Soc., Geophys. Suppl.*, **4**, 143-157, 158-164, 317-331, 332-337, 469-471.

Chen, Q. F., and Willemann, R. J. (2001). Global test of seismic event locations using three dimensional Earth models. *Bull. Seism. Soc. Am.*, **91**, 6, 1704-1716.

Dewey, J. W. (1972). Seicmicity and tectonics in western Venezuela. *Bull. Seism. Soc Amer.***, 62**, 1711-1751.

Dewey, J. W., and Algermissen, S. T. (1974). Seismicity of the Middle America arc-trench system near Managua, Nicaragua. *Bull. Seism. Soc Amer.***, 64**, 1033-1048.

Di Giovambattista, R., and Barba, S. (1997). An estimate of hypocenter location accuracy in a large network, possible implication for tectonic studies in Italy. *Geophys. J. Int*., **129,** 124-132.

Doornbos, D. J. (Ed.) (1988a). Seismological algorithms, Computational methods and computer programs. *Academic Press*, New York, xvii + 469 pp.

Dornboos, D. J. (1988b). Asphericity and ellipticity corrections. In: Dornboos (1988a), 75-85.

Douglas, A. (1967). Joint hypocenter determination. *Nature*, **215**, 47-48.

Dziewonski, A. M., and Gilbert, F. (1976). The effect of small, aspherical perturbations on travel times and a re-examination of the corrections for ellipticity. *Geophys. J. R. astr. Soc.* **44**, 7-17.

Engdahl, E. R., Van der Hilst, R. D., and Buland, R. P. (1998). Global teleseismic earthquake relocation with improved travel times and procedures for depth determination. *Bull. Seism. Soc. Am.,* **88**, 722-743.

Engdahl, E. R., Bondar, I., Bergmann, E., and Firbas, P. (2001). IASPEI Working group on reference events: 1999-2001 activity report.

Evernden, J. F. (1969). Identification of earthquakes and explosions by use of teleseismic data. *J. Geophys. Res.,* **74**, 3828-3856.

Font, Y., Kao, H., Lallemand, S., Liu, C.-S. , and Chiao, L.Y. (2004). Hypocentre determination offshore of eastern Taiwan using the Maximum Intersection method. *Geoph. J. Int.,* **158**, 655-675.

Geiger, L. (1910). Herdbestimmung bei Erdbeben aus den Ankunftszeiten. *Nachrichten von der Königlichen Gesellschaft der Wissenschaften zu Göttingen*, Mathematisch-Physikalische Klasse, 331-349. (In 1912 translated to English by Peebles, F. W. L., and Corey, A. H.: Geiger, L. (1912). Probability method for the determination of earthquake epicenters from the arrival time only. *Bulletin St. Louis University*, **8**, 60-71).

Gutenberg, B., and Richter, C. F. (1933). Advantages of using geocentric latitude in calculating distances. *Gerl. Beitr. Geophysik***, 40**, 380-389.

Gutenberg, B., and Richter, C. F. (1936). Materials for the study of deep-focus earthquakes. *Bull. Seism. Soc. Am.,* **26**, 341 – 390 (edition in French: Données relatives a l'étude des tremblements de terre a foyer profond. *Publications du Bureau Central Séismologique International*, Série **A**, Travaux Scientifiques **15**, 1 - 70, 1937).

Gutenberg, B., and Richter, C. F. (1937). Materials for the study of deep-focus earthquakes (second paper). *Bull. Seism. Soc. Am*., **27**, 157 – 183 (partly edited in French: Données relatives a l'étude des tremblements de terre a foyer profond. *Publications du Bureau Central Séismologique International*, Série **A**, Travaux Scientifiques **15**, 1 - 70, 1937).

Herrin, E. and Taggart, J. (1968). Source bias in epicenter determinations. *Bull. Seism. Soc. Am.,* **58,** 1791–1796.

Horiuchi, S., Negishi, H., Abe, K., Kamimura, A., and Fujinawa, Y. (2005). An automatic processing system for broadcasting earthquake alarms. *Bull. Seism. Soc. Amer*., **95**, 708-718.

Jacob, K. H. (1972). Global tectonic implications of anomalous seismic P travel-times from the nuclear explosion Longshot. *J. Geophys. Res.,* **77**, 14.

Jeffreys, H., and Bullen, K. E. (1940, 1948, 1958, 1967, and 1970). Seismological Tables. British Association for the Advancement of Science, *Gray Milne Trust*, London, 50 pp.

Kennett, B. L. N. (1992). Locating oceanic earthquakes - the influence of regional models and location criteria. *Geophys. J. Int.*, **108**, 848-854.

Kennett, B. L. N. (Ed.) (1991). IASPEI 1991 Seismological Tables. Research School of Earth Sciences, Australian National University, 167 pp.

Kennett, B. L. N., and Engdahl, E. R. (1991). Traveltimes for global earthquake location and phase identification. *Geophys. J. Int*., **105**, 429-465.

Kennett, B. L. N., and Gudmundsson, O. (1996). Ellipticity corrections for seismic phases, *Geophys. J. Int*., **127**, 40-48.

Kennett, B. L. N., Engdahl, E. R., and Buland, R. (1995). Constraints on seismic velocities in the Earth from traveltimes. *Geophys. J. Int*., **122**, 108-124.

Kikuchi, M., and Fukao, Y. (1987). Inversion of long-period P-waves from great earthquakes along subduction zones. *Tectonophysics*, **144**, 231-247.

Kissling, E. (1988). Geotomography with local earthquake data. Rev. Geophys., **26**, 659-698.

Kissling, E., Ellsworth, W. L., Eberhart-Philips, D., and Kradolfer, U. (1994). Initial reference models in local and regional earthquake tomography. *J. Geophys. Res*., **99**, 19635-19646.

Klein, F. (2002). User's Guide to HYPOINVERSE-2000, a Fortran program to solve for earthquake locations and magnitudes, *USGS, Open File Report* **02-171**,123pp.

Klein, F. W. (1978). Hypocenter location program HYPOINVERSE. *U.S. Geol. Surv. Open-File Report.* **78-694**.

Klein, F. W. (1985). HYPOINVERSE, a program for VAX and professional 350 computers to solve the earthquake locations. *U.S. Geological Survey Open-File Report* **85-515**, 53 pp.

Klein, F. W. (2003). The HYPOINVERSE2000 earthquake location program. In: Lee, W. H. K., Kanamori, H., Jennings, P. C., and Kisslinger, C. (Eds.) (2003), 1619-1620.

Lahr, J. C. (1989). HYPOELLIPSE/Version 2.0: A computer program for determining local earthquakes hypocentral parameters, magnitude, and first motion pattern. *U.S. Geological Survey Open-File Report* **89-116**, 92 pp.

Lahr, J. C. (2003). The HYPOELLIPSE earthquake location program. In: Lee, W. H. K., Kanamori, H., Jennings, P. C., and Kisslinger, C. (Eds.) (2003), 1617-1618.

Lay, T., and Wallace, T. C. (1995). Modern global seismology. ISBN 0-12-732870-X, *Academic Press*, 521 pp.

Lee, W. H. K., and Lahr, J. C. (1975). HYPO71 (revised): A computer program for determining hypocenter, magnitude and first motion pattern of local earthquakes. U.S. Geological Survey Open-File Report 75-311, 116 pp.

Lee, W. H. K., Lahr, J. C., and Valdes, C. M. (2003). The HYPO71 earthquake location program. In: Lee, W. H. K., Kanamori, H., Jennings, P. C., and Kisslinger, C. (Eds.) (2003), 1641-1642.

Lee, W. H. K., Kanamori, H., Jennings, P. C., and Kisslinger, C., (Eds.), (2003). "International Handbook of Earthquake and Engineering Seismology, Part B", *Academic Press, Amsterdam*, 1012 pp and 2 CD-ROMs.

Lienert, B. R. E. (1991). Report on modifications made to Hypocenter. *Institute of Solid Earth Physics, University of Bergen*.

Lienert, B. R. E. (1997). Assessment of earthquake location accuracy and confidence region estimate using known nuclear tests. *Bull. Seism. Soc. Am.*, **87**, 5, 1150-1157.

Lienert, B. R. E., and Havskov, J. (1995). A computer program for locating earthquakes both locally and globally. *Seism. Res. Lett.*, **66**, 26-36.

Lienert, B. R. E., Berg, E., and Frazer, L. N. (1988). HYPOCENTER: An earthquake location method using centered, scaled, and adaptively least squares. *Bull. Seism. Soc. Am.*, **76**, 771-783.

Lomax, A. (2005). A reanalysis of the hypocentral location and related observations for the great 1906 California earthquake. *Bull. Seism. Soc. Amer.*, **95**, 861-877.

Lomax, A.,Virieux, J., Volant, P., and Berge, C. (2000). Probabilistic earthquake location in 3D and layered models: Introduction of a Metropolis-Gibbs method and comparison with linear locations. In: Thurberand, C. H., and Rabinowitz, N. (2000). Advances in Seismic Event Location. *Kluwer, Amsterdam*, 101-134.

Lomax, A., Zollo, A., Capuano, P., and Virieux, J. (2001). Precise, absolute earthquake locations under Somma-Vesuvius volcano using a new three-dimensional velocity model. *Geophys. J. Int.* **146**, 313-331.

Morelli, A., and Dziewonski, A. M. (1993). Body wave traveltimes and a spherically symmetric P- and S-wave velocity model, Geophys. J. Int., **112**, 178-194.

Müller, G. (1977). Earth flattening approximation for body waves derived from geometric ray theory - improvements, corrections and range of applicability. *J. Geophys.*, **44**, 429-436.

Nicholson, T., Gudmundsson, Ó., and Sambridge, M. (2004). Constraints on earthquake epicentres independent of seismic velocity models. *Geophys. J. Int.*, **156**, 648-654.

Parolai, S., Trojani, L., Monachesi, G., Frapiccini, M., Cattaneo, M., and Augliera, P. (2001). Hypocenter location accuracy and seismicity distribution in the Central Apennines (Italy). *J. Seism.*, **5**, 243-261.

Pujol, J. (2000). Joint event location – the JHD technique and applications to data from local networks. In: Thurber Rabinowitz(2000), 163-204.

Pujol, J. (2003). Software for joint hypocentral dtermination using local events. In: Lee, W. H. K., Kanamori, H., Jennings, P. C., and Kisslinger, C. (Eds.) (2003), 1621-1623.

Pujol, J. (2004). Earthquake location tutorial: graphical approach and approximate epicentral location techniques. Seism. Res. Lett., **75**, 63-74.

Ringdal, F., and. Kennett, B. L. N (Eds.) (2001). Special issue: Monitoring the Comprehensive Nuclear-Test-Ban Treaty: Source location. *Pure appl. Geophys.*, **158**, (1/2), 1-419.

Roberts, R. G., Christofferson, A., and Cassedy, F. (1989). Real time event detection, phase identification and source location using single station 3 component seismic data and a small PC. *Geophys. J.*, **97**, 471-480.

Rosenberger, A. (2009). Arrival-time order location revisited. *Bull. Seism. Soc. Amer.*, **99**, 2027-2034.

Ružek, B., and Kvasnička, M. (2001). Differential evolution algorithm in earthquake hypocenter location. *Pure appl. geophys.*, **158**, 667-693.

Saari, J. (1991). Automated phase picker and source location algorithm for local distances using a single three-component seismic station. *Tectonophysics*, **189**, 307-315.

Sambridge, M. S., and Kennett, B. L. N. (1986). A novel method of hypocentre location. *Geophys. J. R. astr. Soc.*, **87**, 679-697.

Sambridge, M. S., and Kennett, B. L. N. (2001). Seismic event location: nonlinear inversion using a neighbourhood algorithm. *Pure appl. Geophys.*, **158**, 241-257.

Satriano, C., Lomax, A., and Zollo, A. (2008). Real-time evolutionary earthquake location for seismic early warning. *Bull. Seism. Soc. Amer.*, **98**, 1482-1494.

Schöffel, H.-J. and Das, S. (1999). Fine details of the Wadati-Benioff zone under Indonesia and its geodynamic implications. *J. Geophys. Res*., **104**, 13101-13114.

Schwartz, S. Y., Dewey, J. W., and Lay, T. (1989). Influence of fault plane heterogeneity on the seismic behavior in southern Kurile Islands arc. *J. Geophys. Res*., **94**, 5637-5649.

Schweitzer, J. (2001). HYPOSAT – An enhanced routine to locate seismic events. *Pure and Appl. Geophys.*, **158**, 277-289.

Schweitzer, J., and Storchak, D. A. (2006). Modernizing the ISC location procedures (editorial). *Phys. Earth Planet. Int*., **158**, 1-3.

Shearer, P. M. (1999). Introduction to seismology. Cambridge University Press, 260 pp.

Smith, G. P., and Ekström, G. (1996). Improving teleseismic event locations using a three-dimensional Earth model. *Bull. Seism. Soc. Am*., **86**, 3, 788-796.

Spallarossa, D., Ferretti, G., Augliera, P., Bindi, D., and Cattaneo, M. (2001). Reliability of earthquake location procedures in heterogeneous areas: synthetic tests in the South Western Alps, Italy. *Phys. Earth Planet. Int*., **123**, 247-266.

Stein, S. (1991). Introduction to seismology, earthquakes and Earth structure. *Lecture notes*, Department of Geological sciences, Northwestern University, USA.

Storchak, D. A., Schweitzer, J., and Bormann, P. (2003). The IASPEI Standard Seismic Phase List. *Seism. Res. Lett.*, **74**, 761-772.

Thurber, C. H., and Engdahl, E. R. (2000). Advances in global seismic event location. In: in Thurber and Rabinowitz (2000), 3-22.

Thurber, C. H., and Kissling, E. (2000). Advances in travel-time calculations for three-dimensional structures. In: Thurber and Rabinowitz (2000), 71-100.

Thurber, C. H., and Rabinowitz, N. (Eds.) (2000). Advances in seismic event location. *Kluwer Academic Publishers*, 266 pp.

Tsai, V. C., Nettles, M., Ekström, G., and Dziewonski, A. (2005). Multiple CMT source analysis of the 2004 Sumatra earthquake. *Geophysical Research Letters*, **32**; L17304, doi: 10.1029/2005GL023813.

Wadati, K. (1933). On the travel time of earthquake waves. Part. II. *Geophys. Mag.* (Tokyo) **7**, 101-111.

Waldhauser, F., and Ellsworth, W. L. (2000). A double-difference earthquake location algorithm: method and application to the northern Hayward fault, California. *Bull. Seism. Soc. Am.*, **90**, 1353-1368.

Wiechert, E. (1907). Über Erdbebenwellen. Theoretisches über die Ausbreitung der Erdbebenwellen. *Nachrichten von der Königlichen Gesellschaft der Wissenschaften zu Göttingen*, Mathematisch-physikalische Klasse, 413-529.